Chapter 2
Molecular Clouds and the Onset of Star Formation

This chapter is concerned with the main physical processes that lead to star formation in gas that has already evolved to the molecular cloud state. Although this material is already relatively cold and dense, in general it has too much magnetic, rotational, thermal, and turbulent energy to allow collapse into low-mass stars. A number of physical processes, however, tend to dissipate these energies, or allow local collapse in spite of them, on time scales up to 10^7 yr. The main effects that need to be considered are heating, cooling, the role of shock waves, magnetic braking of rotation, diffusion of the magnetic field with respect to the gas, and the generation and decay of turbulence. After a review of the general properties of molecular clouds, the chapter discusses the physical processes relevant to the phase known as "star formation" (Table 1.1). It then discusses three important scenarios: magnetically controlled star formation, turbulence-controlled star formation, and induced star formation.

2.1 Molecular Cloud Properties

The molecular gas in the galaxy exhibits structure over a wide range of scales, from 20 pc or more in the case of giant molecular clouds down to 0.05 pc for molecular cloud cores. The clouds have been characterized as both clumpy and filamentary. The general properties on selected scales are listed in Table 2.1. In fact each type of structure exhibits a range of properties [335]. The clumpiness of a molecular cloud can be characterized by a so-called *volume filling factor* f_f. If a component of a molecular cloud has a particle density n (in cm^{-3}) which is greater than $< n >$, the average density of the molecular cloud as a whole, then $f_f =< n > /n$. Thus roughly f_f is the probability that the matter has density n. On the molecular core scale, where $n > 10^5$, and where star formation is believed to occur, this factor is only about 0.001. In addition to the listed properties, the structures on various scales exhibit rotation and magnetic fields, which are discussed in later sections of this chapter.

P.H. Bodenheimer, *Principles of Star Formation*, Astronomy and Astrophysics Library,
DOI 10.1007/978-3-642-15063-0_2, © Springer-Verlag Berlin Heidelberg 2011

Table 2.1 Properties of molecular clouds

	Giant molec. cloud	Molecular cloud	Molecular clump	Cloud core
Mean radius (pc)	20	5	2	0.08
Density n(H_2) (cm^{-3})	100	300	10^3	10^5
Mass ($M_\odot$)	10^5	10^4	10^3	10^1
Linewidth ($km\,s^{-1}$)	7	4	2	0.3
Temperature (K)	15	10	10	10

On the giant molecular cloud scale, given an approximate mass one can calculate the gravitational potential energy and find that it is far greater in absolute value than the thermal energy. Thus the clouds are certainly highly gravitationally bound, but in general they are not collapsing. The linewidths in CO (several km/s) are always greater than the thermal width at 10 K (full width at half maximum of 0.13 km/s for CO), implying that some other mechanism, such as turbulence or magnetic fields, is helping to support the cloud against gravity. In fact, if these linewidths are caused by turbulence and/or magnetic fields, the deduced energies are close to sufficient to support the clouds. Inside molecular clouds, the gas pressures are higher than those in the surrounding interstellar medium, and almost all molecular clouds in our galaxy exhibit star formation. The deduced mean lifetime of molecular clouds is 10 Myr (subject to considerable argument). The suggested mechanism for breakup and destruction of the clouds is ionization effects from the most massive stars, particularly near the edge of the cloud, where the hot gas in the ionized region drives a flow of material away from the cloud. Evidence for this value of the age is provided by the fact that intermediate age clusters, with ages >10 Myr, do not have associated molecular material. By means of a similar method, the typical lifetime of a molecular cloud in the Large Magellanic Cloud is estimated to be 27 Myr $\pm 50\%$ [59].

Although the main constituents of molecular clouds are molecular hydrogen and atomic helium, it is very difficult to observe spectral lines of these species because the required excitation conditions do not exist, except possibly under special conditions, such as shocks. That is, the equivalent temperature needed to lift H_2 molecules to their lowest excited states, so they can emit a photon, is 512 K. Instead, trace species are used, in particular, emission lines of CO. The abundance of CO relative to H_2 is estimated to be about 10^{-4}, but with considerable uncertainty. The molecule can be observed in three different forms: $^{12}C^{16}O$, $^{13}C^{16}O$, and $^{12}C^{18}O$, the first of which is usually optically thick in molecular clouds, the second of which is marginally so, and the third of which is optically thin. At the higher densities in molecular clouds ($n \geq 10^5\,cm^{-3}$) CO ceases to be a reliable estimator of the density of H_2, in part because the lines become optically thick, and in part because the CO tends to freeze out on grain surfaces at high densities, so that the gas phase is depleted [13].

To measure masses and densities, the main observed quantity is the particle column density N, that is, the number of molecules along the line of sight through,

say, a clump, divided by the projected area of the clump. To measure this quantity one needs an optically thin line, so that radiation from all molecules emitting that line is seen; on the larger scales $^{13}C^{16}O$ is often used for this purpose. The mechanism for production of the line radiation is collisional excitation of a low-lying level (for CO the equivalent excitation temperature is around 5 K) by the dominant molecular H_2, followed by radiative de-excitation; thus the strength of the line, integrated over the line profile (that is, over all velocities in the line) is proportional to the local emitting particle density. The details of the complicated and somewhat uncertain conversion from line emission to column density of $^{13}C^{16}O$, and then from column density of $^{13}C^{16}O$, to total column density $N_{\rm tot}$, are given in [481]. Then the size of the clump is estimated from the linear scale of the region over which the line intensity drops by a factor e. Given the distance, the mass then follows from

$$M = \int m N_{\rm tot} dA \tag{2.1}$$

and the mean number density n (particles per unit volume) is obtained from

$$n = \frac{M}{mV} \approx \frac{3N_{\rm tot}}{4R} \tag{2.2}$$

where m is the mean particle mass, V is the total volume, and R is the radius. The dimension of the cloud along the line of sight is not observed, but one assumes the cloud is spherical or cylindrical with length along the line of sight comparable to the linear dimension on the plane of the sky. Thus the typical column density of a molecular clump, with $n \approx 10^3\,{\rm cm}^{-3}$ and a radius of 2 pc is 8×10^{21} particles per $\rm cm^2$. An example of an observation in CO is given in Fig. 2.1.

There is a fundamental limitation to the use of a given molecule such as CO as a density probe, related to the concept of "critical density", defined as

$$n_{\rm crit} = \frac{A_{ij}}{\gamma_{ij}} \tag{2.3}$$

where A_{ij} is the Einstein probability for the radiative downward transition $i \rightarrow j$ per particle in level i per unit time, and $n\gamma_{ij}$ is the probability of a downward collisionally-induced transition per particle in level i per unit time. The critical density is that where the two probabilities are equal ($\gamma_{ij} n_{\rm crit} = A_{ij}$). Thus at densities above $n_{\rm crit}$ the line intensity is no longer clearly related to the density, because the collisionally induced transition produces no photon. For the $J = 1 \rightarrow 0$ transition in CO, $n_{\rm crit} = 3 \times 10^3$ particles $\rm cm^{-3}$. In practice, a given transition is a good probe of regions somewhat below or near the critical density, but not above it.

Thus on the clump scale (Table 2.1) the $^{12}C^{16}O$ is near $n_{\rm crit}$ and it is useful for picking out density peaks on that scale (Fig. 2.1). But in general, no single observational tracer can represent a molecular cloud on all scales. For clumps, $^{13}C^{16}O$ or $^{12}C^{18}O$ can be used because of their much lower abundance relative to $^{12}C^{16}O$. On the even smaller scales of cores (0.05–0.1 pc), density can be traced

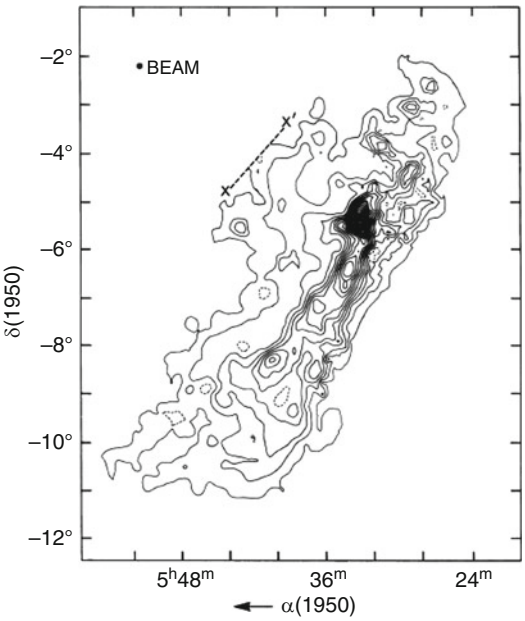

Fig. 2.1 Contours of equal intensity on the plane of the sky in the Orion A cloud. The transition is the $J = 1 \rightarrow 0$ in the $^{12}C^{16}O$ molecule at 2.6 mm. The intensity is integrated over the line width. The *dark region* is the star-forming dense gas associated with the Orion Nebula; it has a radius of roughly 2 pc. Reproduced, by permission of the AAS, from [337]. © The American Astronomical Society

by a transition in CS at 3.1 mm ($n_{\text{crit}} = 4.2 \times 10^5$) and one in H_2CO at 2.1 mm ($n_{\text{crit}} = 1.3 \times 10^6$).

Another way of getting the column density in a region is to use visual extinction of starlight by intervening dust. Dust, in the form of small particles with characteristic size 0.1–0.2 μm, accounts for about 1% of the mass of interstellar material. For example, there is an empirical relation

$$A_v = (N_H + 2N_{H_2})/2 \times 10^{21} \tag{2.4}$$

where the extinction A_v is given in magnitudes, N_H is the column density in particles cm^{-2} for atomic hydrogen, and N_{H_2} is the column density in molecular hydrogen [70]. To calibrate this relation, the quantity N_H is obtained, via satellite observations, from the strength of Lyα absorption of light from hot OB stars by material in intervening clouds, while N_{H_2} is obtained similarly from absorption in the Lyman molecular bands. Then A_v is obtained from the reddening of the light, also from the OB stars. The dust also provides thermal radiation at the dust temperature; this continuous spectrum in the 1 mm wavelength range, provides a nice complement to the molecular line radiation. The dust temperature, which is

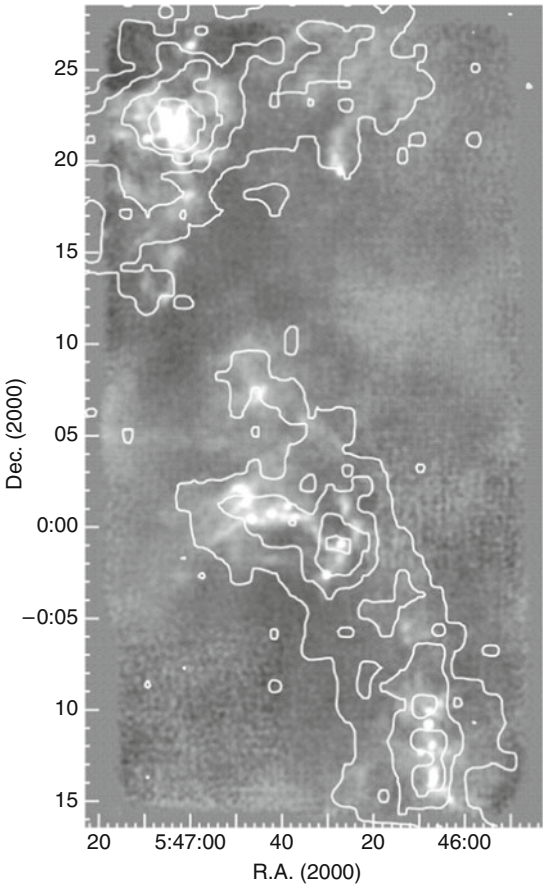

Fig. 2.2 Observed structure of a portion of the Orion B molecular cloud, both in the continuum at 850 μm (grey scale) and in a molecular transition of CS (contours). The bright spots in the continuum, an indicator of high dust density, correspond in general to the highest contours in CS emission, an indicator of high gas density. Those peaks have a size scale of ≈0.1 pc, and would be considered "cores", with masses in the range 0.2–12 $M_{\odot}$. Reproduced by permission of the AAS from [243]. © The American Astronomical Society

determined from analysis of the properties of the far infrared/millimeter emission as a function of wavelength, may be different from the gas temperature, which is determined from the relative strengths of molecular emission lines arising from energy levels of different excitation energy. Particularly at the lower densities, the gas and dust are not well coupled by collisions, and the physical processes that determine their equilibrium temperature are different. Figure 2.2 shows observations of cores both from continuum 850 μm observations of the dust and molecular line emission which traces the gas. The scale of the figure (top to bottom) is approximately 4 parsec. Cloud cores can also be observed by visual extinction of

Fig. 2.3 The Cone nebula, in the star-forming region NGC 2264, taken by the Advanced Camera for Surveys (ACS) on Hubble Space Telescope, April 2, 2002. The portion of the dark nebula that is shown measures about 0.8 parsec in length. Credit: NASA, H. Ford (JHU), G. Illingworth (UCSC), M. Clampin (STScI), G. Hartig (STScI), the ACS Science Team, and ESA

starlight (Fig. 3.2). Figure 2.3 shows a related observation of a clump-scale object that is being eroded by ionizing radiation from O and B stars. In this case the cold molecular gas and dust extinct the optical radiation of the background ionized region produced by the nearby hot O star S Monocerotis in the young cluster NGC 2264.

A number of well-defined relationships arise from the data, including the linewidth-size relation, the condition of near virial balance, and the mass spectrum (number of objects per unit mass interval as a function of mass). If the CO line widths are determined as a function of scale, a well-defined linewidth-size relation appears, as first determined by Larson [301]. Over a scale range (L) of 0.05–60 pc, he found $\Delta v \approx L^{0.38}$ where L is given in pc and Δv is the observed full width of a spectral line at half maximum, in km s^{-1} (see Fig. 2.4). This relation is similar to what one would expect for laboratory incompressible turbulence, which gives the so-called Kolmogorov spectrum with the exponent 1/3. Subsequent studies have confirmed the existence of the linewidth-size relation, but there is appreciable scatter in the data, and various determinations [224, 312, 475] give power law exponents ranging from 0.4 to 0.6, depending on the details of how velocities and sizes are measured. In view of the uncertainty, a value of 0.5 is commonly used. At the low-mass core scale (0.1 pc), the linewidth-size relation changes, so that there is no longer any significant correlation between linewidth and size [191]. On this scale, the line widths are usually dominated by the thermal component,

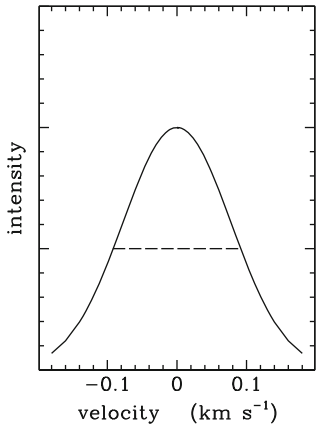

Fig. 2.4 Sketch of a molecular emission line, giving intensity in arbitrary units as a function of velocity in the line of sight. Zero velocity corresponds to the rest wavelength at the center of the line. The linewidth Δv is measured according to the dashed line. The line strength is the intensity integrated over all velocities. The profile shown is assumed to be a Gaussian. If it is assumed to arise only from thermal motions of the molecule, then $\Delta v_{\rm th} = [8k_B T(\ln 2)/m]^{1/2}$, where m is the mass of the molecule in grams and k_B is the Boltzmann constant. In the figure, for the case of the ammonia molecule NH_3, the measured $\Delta v = 0.188$ km s^{-1} corresponds to a temperature of 13 K. Note that the velocity dispersion, namely the isothermal sound speed or equivalently the root mean square of the velocity of a particle in one dimension, $\sigma_{\rm th} = (k_B T/m)^{1/2} = \Delta v/2.355$. If turbulence is also present, then the linewidth $\Delta v^2_{\rm tot} = \Delta v^2_{\rm th} + \Delta v^2_{\rm turb}$ where $\Delta v_{\rm turb} = 2.355\sigma_x$ and σ_x is the one-dimensional turbulent velocity dispersion, which is independent of the particle mass

$\Delta v/\Delta v_{therm} \approx 1.3$, so the non-thermal component, while still present, is now subsonic.

It is not clear exactly what this relation means. The standard interpretation is that some kind of compressible, highly supersonic, turbulence could be present, with properties somewhat different from laboratory turbulence (lab turbulence is subsonic). Under this basic assumption, one can approximately state Larson's findings (often referred to as "Larson's Laws") as follows. The first is the linewidth-size relation [475]:

$$\sigma_x \approx (0.7 \pm 0.07) R_{pc}^{0.5\pm0.1} \ \ {\rm km\ s^{-1}} \tag{2.5}$$

where σ_x is the one-dimensional velocity dispersion, in this case the mean turbulent velocity measured in the line of sight, and R is approximately the radius of the cloud. Clearly on all scales larger than about 0.1 pc, the turbulence is supersonic, because the thermal velocity dispersion at 10 K is 0.19 km s^{-1} for a gas with mean molecular weight 2.37 (approximately 70% H and 28% He by mass).

The second finding is essentially that molecular clouds and clumps within them are gravitationally bound and are close to virial equilibrium. The Virial Theorem for a quasi-spherical cloud in force balance can be written

$$2E_{\rm kin} + 2E_{\rm th} + E_{\rm mag} - 3P_{\rm surf}V + E_{\rm grav} = 0. \tag{2.6}$$

where $E_{\rm kin}$ is the total macroscopic kinetic energy, including rotation and turbulence, $E_{\rm th}$ is the total thermal energy, $E_{\rm mag}$ is the total magnetic energy (magnetic surface terms are not considered here), $E_{\rm grav}$ is the total gravitational energy, $P_{\rm surf}$ is the external pressure, and V is the total volume. Assuming that the kinetic energy is dominated by turbulence, that the only other term of importance is $E_{\rm grav}$, and that the cloud can be approximated by a uniform-density sphere with mass M, then the Virial Theorem gives

$$M\sigma^2 = \frac{3}{5}\frac{GM^2}{R} \tag{2.7}$$

where the three-dimensional velocity dispersion σ is related to σ_x by $\sigma^2 = \sigma_x^2 + \sigma_y^2 + \sigma_z^2$. Assume isotropic velocities and solve for the mass, which is denoted by the virial mass $M_{\rm vir}$:

$$M_{\rm vir} = \frac{5\sigma_x^2 R}{G}. \tag{2.8}$$

For an actual cloud one defines $\alpha_{\rm vir} = M_{\rm vir}/M$, so that a cloud with $\alpha_{\rm vir} = 1$ is in virial balance but not necessarily in hydrostatic equilibrium, because of the assumption regarding uniform density. But if $\alpha_{\rm vir} < 1$ then the cloud is definitely not in force balance and is unstable to collapse.

Note that the mean column density $\bar{N}_H = M/(\pi m R^2)$, where m is the mean mass (in grams) per particle and R is the radius of a clump, so that $\sigma^2 \propto \bar{N}_H R$, so $\bar{N}_H$ = const. (there is some observational evidence in support of this but the suggestion of virial equilibrium according to (2.8) is oversimplified). The conclusion that all molecular clouds have similar column densities, on all length scales where the linewidth-size relation applies, is Larson's third finding, even though it can be derived from the first two. One can also deduce from Larson's findings that $M \propto R^2$ and $\rho \propto R^{-1}$.

Another explanation of Larson's findings [459] is that they represent virial equilibrium of masses on various scales with the magnetic field supporting the region against gravity. The linewidth in that case would arise from Alfvén waves, and it can easily be shown that $\Delta v \propto R^{0.5} B^{0.5}$ (see below).

The mass spectrum of the molecular clouds, clumps and cores has been measured over a wide range of masses by several different methods. The results are usually expressed in terms of a power law

$$dN/dM = \text{const.} \times M^{-x} \tag{2.9}$$

where dN is the number of clouds in the mass range M to $M + dM$. On the largest scales, corresponding to giant molecular clouds in the mass range above about $3{\times}10^4\,{\rm M}_\odot$, the preferred method is to use the total luminosity in a spectral line of ^{12}CO or ^{13}CO as an indicator of mass. The latter molecule is preferred because it is usually optically thin, but the former is often used simply because its intensity is greater. In either case corrections must be applied [352] to convert from molecular column density to total mass. The typical result [552] is $x \approx 1.6$ with an upper mass cutoff at about $6 \times 10^6\,{\rm M}_\odot$.

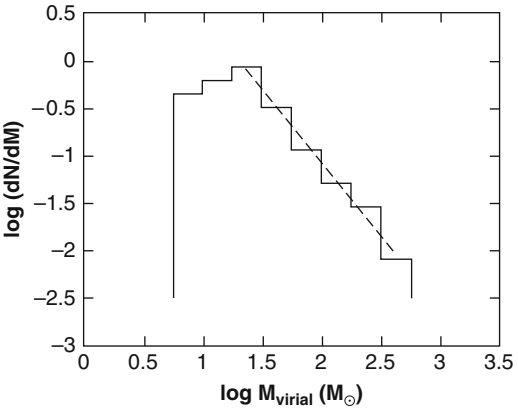

Fig. 2.5 Mass spectrum of clumps in the L1630 molecular cloud (Orion B). The spectrum is plotted as a function of the virial mass in solar masses. The *dashed line* represents a slope of −1.6. Below about 20 $M_\odot$ the observations are incomplete. Reproduced by permission of the AAS from [293]. © The American Astronomical Society

On smaller scales, one can use line widths and sizes of various regions to get $M_{\rm vir}$ from (2.8). An example of such a mass spectrum obtained by use of the CS molecule in the Orion region, in the mass range 20–500 $M_\odot$, is shown in Fig. 2.5, where the power-law index is also $x = 1.6$. This spectrum does not match that of stars, which if fitted to a power law in the mass range 2–10 $M_\odot$, has an exponent of about –2.3. The diagram shown represents clumps in the Orion region; however very similar relations are obtained in different molecular clouds and with different line tracers; the power law seems to hold in a wide range of masses. However there is somewhat of a range in the power laws deduced, so a better representation of the situation would be that x falls in the range 1.3–1.9 [335]. Still, the power law in the clump mass spectrum is consistent with that for molecular clouds as a whole.

At even lower masses, in the core-mass range, a somewhat different result is obtained by a different method [19, 370]. Continuum dust emission at 1.3 mm is used to estimate actual masses (rather than virial masses). The flux in the (optically thin) millimeter continuum can be converted, using a standard dust-to-gas ratio, to column density N_H and then to total mass (the method is described in more detail in Chap. 4). The observations show that pre-stellar condensations in the Rho Ophiuchi region follow approximately $dN/dM \propto M^{-1.5}$ below 0.5 $M_\odot$, but above that mass it steepens to $dN/dM \propto M^{-2.5}$. This observation (which has been confirmed by other studies) is not too different from the stellar mass spectrum, which gives $dN/dM \propto M^{-2.3}$ for masses above 0.5 $M_\odot$ but $dN/dM \propto M^{-1.3}$ for lower masses. The switch in slopes occurs at about 0.6 $M_\odot$, at about the same mass where a corresponding change occurs in the stellar mass spectrum. There is a factor 2 uncertainty in core masses, and it is not entirely clear that the slope change is not due to some selection effect, but this result suggests that the IMF for stars in clusters is determined at the pre-stellar stage.

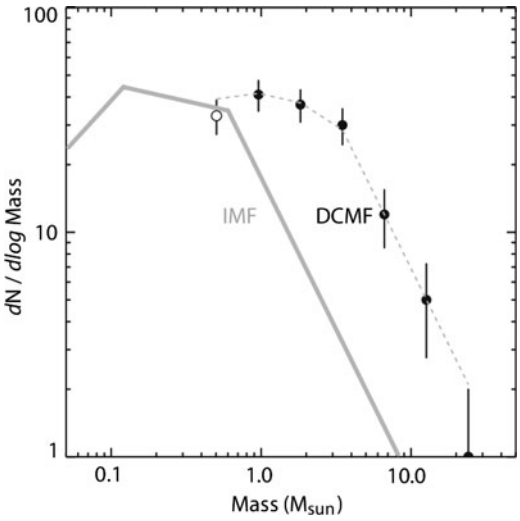

Fig. 2.6 Mass function of dense molecular cores in the Pipe Nebula (*filled circles*), compared with the initial mass function for stars in the Orion Nebula cluster (*grey line*). The *dashed line* refers to the stellar mass function shifted to higher masses by a factor of about 4. Credit: J. F. Alves, M. Lombardi, C. J. Lada: *Astron. Astrophys.* **462**, L17 (2007), reproduced with permission. © European Southern Observatory

An independent method for the core mass function [15] involves observations of the nearby (130 pc) molecular cloud known as the Pipe Nebula, whose background consists of large numbers of stars in the Galactic bulge. By measuring the near IR extinction of those background stars caused by the dust in low-mass dense cores in the Pipe Nebula, one can obtain the mass of each core, using the standard conversion (2.4) between extinction in magnitudes and hydrogen column density N_H. The results are shown in Fig. 2.6 (note that the mass function, not the mass spectrum, is plotted). The advantage of this method is that it avoids the uncertainties in the determination of masses through dust emission. The typical core measured here has density $\sim 10^4$ particles/cm^3. The broad grey line is the stellar IMF as measured in the Orion Nebula cluster. The circles with error bars are the mass function determined in the dense cores. The dotted grey line is the stellar IMF shifted over by a factor 4 in mass. Clearly the shape of the mass function of the dense cores is very similar to that of the stars and the change in slope at lower masses is evident; the change in slope occurs at 2–3 $M_\odot$, rather than about 0.6 $M_\odot$ for the IMF. If a correction for background extinction is made then the difference in mass between the two curves reduces to a factor 3. The conclusion is that the stellar IMF is set by the mass function of dense cores, and there is an efficiency factor of about 30% in the process of turning the mass of the core into a star. This conclusion is supported theoretically by a calculation [460] that includes the effects of magnetic fields and outflows and which also shows an efficiency of about 30%.

2.2 Initial Conditions for Star Formation

The requirement on a region in a molecular cloud that must be satisfied before it can collapse and form a star was first derived by Sir James Jeans [241]. His method was a linear stability analysis performed on the basic hydrodynamic equations, assuming an isothermal gas (Problem 2), including only thermal and gravitational effects. A simpler method of defining the initial conditions for collapse, which, however, includes all relevant physical effects, is to require that the absolute value of the gravitational energy must exceed the sum of the thermal, rotational, turbulent, and magnetic energies. This requirement defines a mass (M) of gas that is gravitationally bound. For this mass to be as small as a solar mass, the requirement can be satisfied only in the coolest, densest parts of the interstellar medium. Thus the requirement is

$$|E_{\rm grav}| > E_{\rm th} + E_{\rm rot} + E_{\rm turb} + E_{\rm mag}. \tag{2.10}$$

For an assumed spherical configuration,

$$E_{\rm grav} = -C_{\rm grav}\frac{GM^2}{R} \tag{2.11}$$

where $C_{\rm grav}$ is a constant depending on the mass distribution and equals 3/5 for uniform density. The total thermal energy for an isothermal ideal gas with temperature T is

$$E_{\rm th} = \frac{3}{2}\frac{R_{\rm g}TM}{\mu} \tag{2.12}$$

where $R_{\rm g} = k_B/m_u$ is the gas constant, k_B is the Boltzmann constant, m_u is the atomic mass unit, and μ is the molecular weight of the gas in atomic mass units. The rotational energy is

$$E_{\rm rot} = C_{\rm rot}MR^2\Omega^2 \tag{2.13}$$

for an assumed uniform angular velocity Ω, where $C_{\rm rot}$ depends on the mass distribution, and equals 1/5 for uniform density. The turbulent kinetic energy is

$$E_{\rm turb} = \frac{1}{2}M\sigma^2 \tag{2.14}$$

where σ is the mean turbulent velocity, as in (2.7). The magnetic energy is given by the volume integral

$$E_{\rm mag} = \frac{1}{8\pi}\int B^2 dV \approx \frac{1}{6}B^2R^3 \tag{2.15}$$

where B is the assumed uniform magnetic field.

Now consider thermal and gravitational effects alone, as did Jeans in his original analysis. Although his analysis contains a physical inconsistency, the result is still very similar to that obtained by energy considerations. The requirement that a uniform-density, uniform-temperature sphere be gravitationally

bound $[(3/5)GM^2/R = (3/2)R_gTM/\mu]$ leads to the determination of the Jeans length:

$$R_J = \frac{0.4GM\mu}{R_gT}, \tag{2.16}$$

where $\mu \approx 2.37$ for solar composition with molecular hydrogen. For a cloud of a given mass and temperature, the radius must be smaller than R_J to be unstable to gravitational collapse. Alternatively, we can eliminate the radius from (2.16) in favor of the density ρ, assuming again that the gas is a sphere, to obtain an expression for the Jeans mass, which is the minimum mass that the cloud of given (ρ, T) must have to be unstable:

$$M_J = \left(\frac{5}{2}\frac{R_gT}{\mu G}\right)^{3/2}\left(\frac{4}{3}\pi\rho\right)^{-1/2} = 8.5\times 10^{22}\left(\frac{T}{\mu}\right)^{3/2}\rho^{-1/2}\ \text{g}. \tag{2.17}$$

Another commonly used version of the Jeans length is obtained by eliminating the mass in (2.16) in favor of density and radius:

$$R_J \approx \left(\frac{R_gT}{\mu}\right)^{1/2}\frac{1}{\sqrt{G\rho}} \approx c_s t_{\text{ff}} \tag{2.18}$$

where c_s is the isothermal sound speed and t_{ff} is defined by (1.1). Here, given T and ρ, the radius of the cloud must be larger than R_J for collapse to occur.

An alternate form of the thermal Jeans mass is known as the *Bonnor–Ebert* mass. The situation envisaged here is slightly different: an isothermal cloud exists in equilibrium, with the effects of the internal pressure gradient, plus an external confining pressure P_{surf}, balancing gravity. Only gravitational effects and thermal effects are considered in the cloud interior. This problem, involving a bounded isothermal sphere, is treated in more detail in Chap. 3, where it is shown that the corresponding critical length for instability to collapse is essentially identical to (2.16).

We now consider rotational effects in addition to thermal effects and gravity. We define $\alpha = E_{\text{th}}/|E_{\text{grav}}|$ and $\beta = E_{\text{rot}}/|E_{\text{grav}}|$, where the density of the sphere and its angular velocity Ω are assumed constant. The revised expression for the Jeans mass becomes

$$M_J = \left(\frac{\frac{3R_gT}{2\mu} + 0.2\Omega^2R^2}{0.6G}\right)^{3/2}\left(\frac{4}{3}\pi\rho\right)^{-1/2}, \tag{2.19}$$

and $M > M_J$ is the condition for the cloud to collapse. Alternatively,

$$\alpha \le 1 - \beta \tag{2.20}$$

for collapse, although numerical studies indicate that actually $\alpha \le 1 - 1.43\beta$ is a more realistic criterion. Clearly rotation has a stabilizing influence, but in the typical observed cloud core β is relatively small (see below). However, even if criterion (2.20) is satisfied and the cloud starts to collapse (assuming conservation of angular

momentum), the rotational energy $E_{\rm rot} = J^2/2I \approx J^2/(MR^2)$, where J is the total angular momentum and I is the moment of inertia, increases faster than the gravitational energy, and the collapse could be stopped at relatively low density.

Rotation is detected in molecular clouds and cloud cores through observations of a gradient in the radial velocity dv/ds, where s is a distance in the plane of the sky. This quantity is measured at various points across the cloud, for example, by the Doppler shifts of emission lines in NH_3 [188, 191]. A linear velocity variation with the spatial coordinate across the cloud is consistent with uniform rotation. From the velocity gradient, and from an assumed model of uniform rotation which is consistent with the observations within the errors, the angular velocity $\Omega \approx dv/ds$ and the specific angular momentum $j \approx 0.4\Omega R^2$ are derived. The inclination angle of the rotation axis to the line of sight is not known. About half of the clouds observed show measurable rotational velocities; the remainder are presumably rotating below the observational limit. On the cloud core scale, typical values of Ω are 10^{-13}–$10^{-14}\,{\rm s}^{-1}$. Rotation has also been detected on larger molecular cloud scales. For example, CO measurements indicate that a gradient in the line-of-sight velocity exists in the Orion A cloud (Fig. 2.1), extending from its upper right end to its lower left end [337], implying rotation about an axis perpendicular to the galactic plane, but in the opposite sense to the Galactic rotation.

Rotation does not appear to be a major factor in the support of clouds against collapse. Nevertheless there is an angular momentum problem, as indicated by the data in Table 2.2. An example of the angular momentum problem was stated by Spitzer [476] as follows: Consider a gas cylinder 10 pc long and 0.2 pc in radius (a filament) with density $5 \times 10^{-23}\,{\rm g\,cm}^{-3}$. Its mass is about a solar mass. Let it rotate about its long axis, say with the typical galactic rotation, $\Omega = 10^{-15}\,{\rm s}^{-1}$. Its contraction parallel to J is not opposed by rotation, but to reach stellar size the radius perpendicular to J must contract by 7 orders of magnitude. Since if angular momentum is conserved $\Omega R^2 =$ constant, Ω must increase by 14 orders of magnitude, to 10^{-1}. The corresponding rotational velocity of the star then would be $6 \times 10^9\,{\rm cm\,s}^{-1}$, or 0.2 c! The centripetal acceleration would be 10^4 times that of gravity.

Table 2.2 Characteristic values of specific angular momentum

Object	J/M ($\rm cm^2\,s^{-1}$)
Binary orbit (10^4 yr period)	4×10^{20}–10^{21}
Binary orbit (10 yr period)	4×10^{19}–10^{20}
Binary orbit (3 day period)	4×10^{18}–10^{19}
100 AU disk (1 $M_\odot$ star)	4.5×10^{20}
T Tauri star (rotation)	5×10^{17}
Jupiter (orbit)	10^{20}
Present Sun (rotation)	10^{15}
Molecular clump (scale 1 pc)	10^{23}
Cloud core (scale 0.1 pc)	1.5×10^{21}

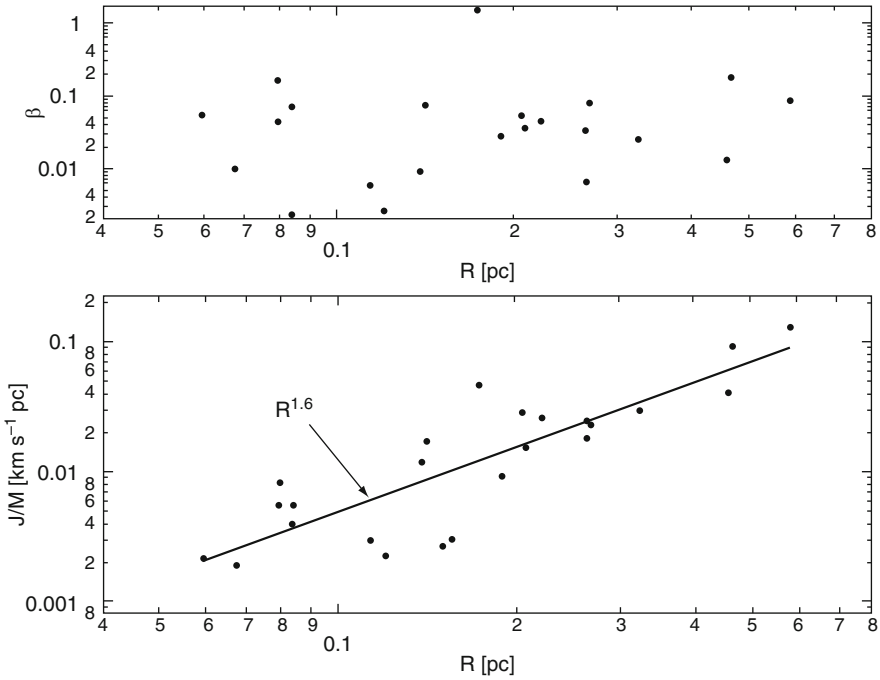

Fig. 2.7 Ratio β of rotational energy to absolute value of gravitational energy (*upper*), and specific angular momentum (*lower*), as a function of the size of a molecular cloud core, based on observations of the velocity gradient across the core. 1 km s^{-1} pc = 3.08 $\times 10^{23}$ cm^2 s^{-1}. Reproduced, by permission of the AAS, from [191]. © 1993 The American Astronomical Society

The results concerning rotation show that first, the angular velocity Ω is similar on all scales; it is only slightly higher in cloud cores than in molecular cloud clumps as a whole, suggesting magnetic coupling between the two regions. Second, $j = J/M$ decreases to smaller scales, also suggesting magnetic braking, but this conclusion is not entirely clear because different mass elements are being sampled. A survey [191] of rotational velocities in cloud cores on scales of 0.06–0.60 pc shows values of $j \sim 6 \times 10^{20}$ to 3×10^{22} cm^2 s^{-1}. A fit to the data gives $j \propto R^{1.6}$, implying $\Omega \propto R^{-0.4}$, where R is the size of the core. The values of β and j derived from observations [191] are shown in Fig. 2.7. Note that β is small on average, only 2 or 3%. But, third, if the cores were to collapse with conservation of angular momentum into disks, they would reach equilibrium with an outer keplerian radius of 180–4,500 AU, comparable in size to many observed disks. The fact that cloud cores contain far too much angular momentum to be compatible with stellar rotational velocities of, for example, T Tauri stars, is demonstrated in Table 2.2.

Turbulent motions are important in molecular clouds, and one can define a turbulent Jeans mass in analogy to the thermal Jeans mass. Equating turbulent energy to gravitational energy

$$M_{\rm turb} = \frac{5\sigma_x^2 R}{2G} \tag{2.21}$$

where σ_x is the turbulent velocity dispersion in the line of sight [see (2.5)]. This mass is clearly closely related to $M_{\rm vir}$, as defined by (2.8), but in that equation the Virial Theorem is used, which accounts for the additional factor 2. For example, in a turbulent core of radius 0.1 pc with a velocity dispersion of 1 km s^{-1} the mass must be above 50 $M_\odot$ for collapse. This situation is appropriate for the formation of massive stars (Chap. 5), but, as mentioned earlier, in low-mass cores the thermal effect dominates.

Finally we consider the magnetic Jeans mass, under the assumption that thermal, turbulent, and rotational effects are unimportant. Using the magnetic energy as simply $E_{\rm mag} = \frac{B^2}{8\pi}\frac{4}{3}\pi R^3$ one obtains instability to collapse in a cloud of density ρ, radius R, and uniform magnetic field B if its mass is greater than M_ϕ, where

$$\begin{aligned} M_\phi &= \frac{BR^2}{(3.6G)^{1/2}} = \left(\frac{5}{18\pi^2 G}\right)^{1/2}\phi = \frac{B^3}{(3.6G)^{3/2}(\frac{4}{3}\pi\rho)^2} \\ &\approx 10^3 M_\odot \left(\frac{B}{30\mu G}\right)\left(\frac{R}{2\rm pc}\right)^2 \end{aligned} \tag{2.22}$$

where ϕ is the magnetic flux. Thus on the clump scale (Table 2.1) where typical measured fields are around 30 μG, the magnetic Jeans mass is close to the clump mass.

If one defines a closed loop threaded by a uniform magnetic field B, the magnetic flux is defined by

$$\phi = \int_S \mathbf{B}\cdot\mathbf{n}\, dA \tag{2.23}$$

where S is the surface enclosed by the loop and $\mathbf{n}$ is the normal to that surface. The magnetic induction equation reads

$$\frac{\partial B}{\partial t} = \nabla\times(\mathbf{v}\times\mathbf{B}) - \nabla\times(\eta_{\rm e}\,\nabla\times\mathbf{B}) \tag{2.24}$$

where $\mathbf{v}$ is the velocity vector and $\eta_{\rm e}$ is the electric resistivity (also referred to as the magnetic diffusivity)

$$\eta_{\rm e} = \frac{c^2}{4\pi\sigma_{\rm e}}\,. \tag{2.25}$$

Here c is the velocity of light and $\sigma_{\rm e}$ is the electric conductivity. The second term on the right-hand side of (2.24) represents the decrease in magnetic field as a result of

Ohmic dissipation. The ratio of the first and second terms is known as the *magnetic Reynolds number*, usually expressed as the dimensionless quantity

$$R_{\rm em} = \frac{vL}{\eta_{\rm e}} \tag{2.26}$$

where L is a characteristic length and v is a characteristic velocity. If $R_{\rm em} \gg 1$, then dissipative effects are negligible. In the interstellar gas, $\sigma_{\rm e}$ is high enough so that indeed $R_{\rm em}$ is very large, so that the second term in (2.24) can be neglected. Then, using the condition $\nabla \cdot \mathbf{B} = 0$ and the Gauss theorem, one can prove that, as the material associated with the loop evolves in time, the flux remains constant, a condition known as *flux-freezing*.

If the cloud is collapsing quasi-spherically, then the magnetic flux $\phi \approx \pi B R^2$ remains constant as the cloud collapses, and (2.22) shows that M_ϕ is constant, that is, it would not be possible for the cloud, for example the $1{,}000\,{\rm M}_\odot$ clump just mentioned, to fragment into smaller masses. Furthermore, under these conditions of quasi-spherical collapse $B \propto \rho^{2/3}$ during collapse. In general, however, if the collapse is not spherical or the field is not frozen in, the field will increase as $B \propto \rho^\kappa$, implying $M_\phi \propto \rho^{-3(2/3-\kappa)}$. As long as $\kappa < 2/3$, M_ϕ decreases on compression, and fragmentation eventually becomes possible. It has generally been believed, on both theoretical and observational grounds, that $\kappa \approx 0.5$. In this case, as a cloud contracts, magnetic energy becomes less important relative to gravitational energy. However an extensive set of measurements [126] suggests that κ is actually higher, closer to 2/3, at densities ranging up to those in molecular cloud cores (Fig. 2.9).

The criterion for collapse in the presence of a magnetic field is often stated as a critical mass-to-flux ratio:

$$\left(\frac{M}{\phi}\right)_{\rm crit} = \frac{0.17}{\sqrt{G}} \tag{2.27}$$

where the constant depends on the details of the geometry. If the ratio of the actual M/ϕ to the critical value is greater than unity, the cloud is *supercritical* and can contract. In the *subcritical* case (ratio < 1), the field dominates, preventing overall contraction; however the cloud can contract in the direction parallel to field lines and become quite flattened (neglecting other effects).

The magnetic field influences the evolution of molecular cloud material in various ways. It is important, first, for at least partial support of the magnetic cloud clumps against collapse. If they were collapsing, the star formation rate would be far higher than currently observed. The typical observed field at the mean clump density is $30\,\mu$G. Consideration of the magnetic energy and turbulent energy in comparison with the gravitational energy indicates that the clumps are unlikely to collapse. The measured magnitude of the field at these early stages leads to the magnetic flux problem. For the same interstellar filament of about $1\,{\rm M}_\odot$ that we considered in connection with the angular momentum problem, suppose it has a magnetic field of $3\,\mu$G (appropriate for the low-density interstellar gas) parallel to the long axis. Then the magnetic flux $\pi B R^2 = \pi \times 3 \times 10^{-6} \times (6 \times 10^{17})^2 \approx \pi \times 10^{30}$. Material

can contract along the magnetic field, and we assume that the contraction across the magnetic field takes place with conservation of flux. The final stellar radius is about 6×10^{10} cm, about 7 orders of magnitude smaller than that of the cloud, so the field must increase by 14 orders of magnitude to 3×10^8 gauss, much higher than observed (the mean field on the solar surface is only 1 gauss) and giving a magnetic energy about the same as the gravitational energy, even if the field is uniform through the star. Despite extensive calculations [318], this difficult problem has not yet been resolved.

A second important effect is the braking of rotation. The field is the most likely mechanism to transport angular momentum out of the dense cores of molecular clouds, as discussed in more detail below. Third, if a region of the cloud is subcritical, then evolution of the region to the point of collapse requires that the field diffuse with respect to the matter. Estimated field diffusion times (3×10^6–10^7 yr) are consistent with the spread of ages of stars in at least some young clusters. This process, known as *ambipolar diffusion*, or plasma drift, is treated in more detail in Sect. 2.6. Finally the suprathermal line widths observed in molecular cloud clumps could be accounted for by the Alfvén waves associated with the field.

It is simple to derive an approximate relation between line width Δv, field strength, and linear scale. Assuming approximate balance between magnetic and gravitational forces:

$$\frac{4}{3}\pi R^3 \frac{B^2}{8\pi} = \frac{GM^2}{R} \tag{2.28}$$

and multiplying and dividing the left-hand side by ρ one obtains

$$V_A^2 \approx \frac{2GM}{R} \approx 2\pi G \Sigma R \tag{2.29}$$

where $\Sigma = M/(\pi R^2)$ is the surface density (in g cm^{-2}), and the Alfvén velocity

$$V_A = \frac{B}{\sqrt{4\pi\rho}}. \tag{2.30}$$

Then from the critical mass-to-flux ratio, and assuming that the Alfvén speed determines the line width

$$\frac{\Sigma}{B} = \frac{0.17}{\sqrt{G}} \tag{2.31}$$

and

$$\Delta v = 0.79(\sqrt{G}BR)^{1/2} \approx 1.23 \left(\frac{B}{30\mu\mathrm{G}}\right)^{1/2} \left(\frac{R}{1\mathrm{pc}}\right)^{1/2} \mathrm{km\,s^{-1}}. \tag{2.32}$$

Figure 2.8 shows a plot [373] of this relation (solid line) compared with the observations of regions where R, B, and Δv have been measured. This interpretation of the line widths is in contrast to the alternative view that they are primarily a result of turbulent broadening. Equation (2.32) can be thought of as the alternate form

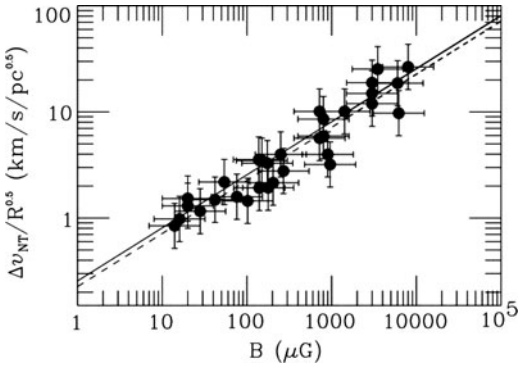

Fig. 2.8 Relationship between the magnetic field, the line width, and the cloud size, as observed (*points with error bars*) and as predicted by (2.32) (*solid line*). The *dashed line* is a fit to the data. The quantity Δv_{NT} is the non-thermal component of the velocity dispersion, in this case caused by magnetic effects. Reproduced by permission of the AAS from [373]. © The American Astronomical Society

of Larson's first finding, when magnetic effects are important. The result strongly suggests that at least in regions where B is strong enough to be measured, the clouds are close to the point where they are magnetically critical.

The evidence for existence of the field is given by measurements of Zeeman splitting of molecular lines. The Zeeman effect is strong enough to be measurable only in certain lines, for example in OH, CN, and the 21 cm line of neutral H. The measurements are extremely difficult, because the Zeeman splitting is only a small fraction of the line width. The goals of such observations are to determine to what extent the magnetic field can support a cloud or clump against collapse, and the relation between field strength and density. In addition, there are measurements of the polarization of starlight [190, 532] which give only the direction of the field but show that the field in a cloud is at least in part well-ordered, rather than random. The Zeeman measurements give only the line-of-sight component of the field, but the results can be deprojected under the assumption of random orientation of the field lines. Relatively few detections exist [125, 126, 166, 510], and in a number of clouds the field has been looked for and not found. Plots of magnetic field against gas density, while subject to large uncertainties in both coordinates, show a general trend that B increases with n with an approximate power law of 0.65 ± 0.05 (Fig. 2.9), as long as the density is above about $300\,\mathrm{cm}^{-3}$; below that value the field does not depend appreciably on density. These data support the following conclusions which apply in cases where there are actual detections of B.

1. The ratio of thermal to magnetic pressures is low, averaging about 0.04.
2. The mass to magnetic flux ratio for the average observed cloud is within a factor 2 of the critical value where gravitational energy and magnetic energy are equal, depending on the assumed geometry. Some observations show that the field is subcritical, others that it is supercritical. However the mean value is supercritical.

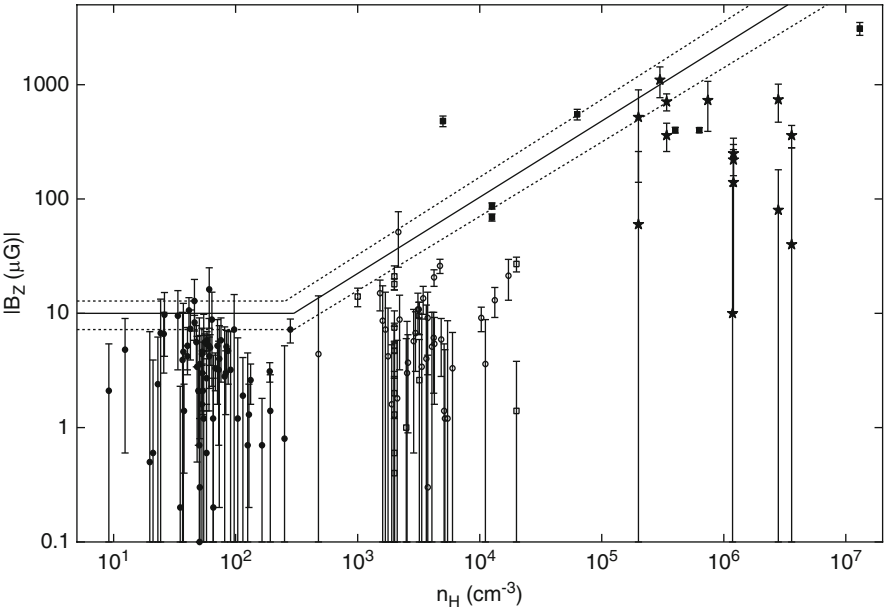

Fig. 2.9 Relationship, in the interstellar gas, between the observed component of the magnitude of the magnetic field in the line of sight $|B_z|$ and the hydrogen volume density in cm^{-3}. In molecular clouds, the horizontal axis is $2n(H_2)$. *Filled circles:* HI diffuse clouds; *open circles:* OH dark clouds; *filled squares and stars:* molecular clouds. The solid line, obtained from a statistical analysis, represents the maximum of the total field strength B as a function of density. In molecular clouds, the actual values of B are randomly distributed between a very small value and this maximum. The dotted lines give the uncertainty in the statistical model. Reproduced by permission of the AAS from [126]. © 2010 The American Astronomical Society

But the large number of non-detections suggests that on the average the magnetic field alone does not prevent material from collapsing.

3. Kinetic energy in macroscopic gas motions is roughly a factor 2 higher than magnetic energy in the average observed cloud. Clouds are in approximate virial balance, with turbulent kinetic plus magnetic energies comparable to gravitational energy (Larson's second finding).
4. At densities above $n \approx 300$ particles cm^{-3}, the maximum magnetic field B scales with density as $|B| \propto \rho^{\kappa}$ with $\kappa \approx 0.65$. This value agrees with the theoretical value of 0.67 for the case in which the cloud is relatively spherical and has a weak magnetic field [362]. However a number of numerical simulations in which the cloud was initially rapidly rotating, e. g. [98], show that the collapse to a disk results in a value for $\kappa \approx 0.5$.

As a specific example, 34 dark-cloud regions were extensively observed [510] with the Arecibo radio telescope in the 1665 and 1667 MHz lines of the

molecule OH. Nine significant detections were made. The number density of H_2 in these regions ranges from 1,500 to 6,600 cm^{-3}. Taking a well-defined set of detections in the range of column densities $N(H_2) = 4 \pm 2 \times 10^{21}\ \mathrm{cm}^{-2}$, the mean magnetic field component in the line of sight is 17 μG, not including the non-detections. We can now estimate the ratio (R) of the observed mass-to-flux ratio to the critical value:

$$R = \frac{(M/\phi)_{\mathrm{obs}}}{(M/\phi)_{\mathrm{crit}}} = \frac{mN\sqrt{G}}{0.17B} = 6 \times 10^{-21} N/B \tag{2.33}$$

where N is the total column density in particles cm^{-2}, m is the mean mass per particle, taken to be 2.4 atomic mass units, taking into account the helium, and B is the magnetic field in μG. The actual magnetic field strength is statistically obtained from the line-of-sight component by multiplying it by a factor 2, and the observed column density of H_2 is corrected by 20% to get N, taking into account the helium. With the very specific set of data chosen, R is very close to 1, perhaps even slightly subcritical. If the cloud region is disk-like rather than spherical, there is an additional small correction which makes R even more subcritical. In view of the uncertainties, the observations do not rule out the picture of magnetically controlled star formation, at least in some regions. However, the large number of non-significant detections or detections showing a very weak field indicate that there are many regions where the magnetic field is not a controlling effect.

Under typical interstellar conditions outside molecular clouds, where the hydrogen is neutral and T $\approx$ 100 K, $n \approx 10$ particles cm^{-3}, and the median field $B \approx 6 \times 10^{-6}$ gauss (Fig. 2.9), the thermal Jeans mass M_J from (2.17) is $10^4\ \mathrm{M}_\odot$, and the magnetic Jeans mass from (2.22) is of the same order of magnitude. The HI (so-called "diffuse") clouds have a wide range of properties; however the typical mass is only $10^3\ \mathrm{M}_\odot$. Thus it is clear that in order to get a region with mass of order $1\ \mathrm{M}_\odot$ to collapse, we must consider regions, in molecular clouds, that are denser and cooler than average. In molecular clumps with temperature 10 K, mean number density of H_2 of $10^3\ \mathrm{cm}^{-3}$, and magnetic field 3×10^{-5} gauss, the thermal Jeans mass (assuming a mass density of $\rho = 3.3 \times 10^{-21}\ \mathrm{g\,cm}^{-3}$ and a mean molecular weight $\mu = 2$) under these conditions is only about $10\ \mathrm{M}_\odot$, while the magnetic Jeans mass and the turbulent Jeans mass (2.22) and (2.21) are both comparable to the clump mass, about $1 \times 10^3\ \mathrm{M}_\odot$. Thus probably turbulence and the magnetic field combine to keep the typical clump from collapsing. In the higher-density cloud cores where masses are a few $\mathrm{M}_\odot$, sizes 0.05 pc, temperature 10 K, and density about $10^5\ \mathrm{cm}^{-3}$, the thermal Jeans mass is down to about $1\ \mathrm{M}_\odot$, and the turbulence is subsonic, so $M_{\mathrm{turb}} < M_J$. The magnetic Jeans mass, assuming that the field strength is roughly 100 μG (Fig. 2.9), is about 2 $\mathrm{M}_\odot$. However here the assumptions of spherical contraction and flux-freezing that led to (2.22) are starting to break down; also not all cores have magnetic fields that strong.

2.3 Heating and Cooling

Star formation is clearly favored in cloud cores where the temperature is only 10 K. But why is the temperature so low? The rates of heating and cooling are important for determining the temperature as a function of density and for maintaining the low temperature of molecular cloud material once it starts to compress under the influence of gravity. The details of the heating and cooling processes are complicated, but the somewhat surprising result is that for densities ranging from the clump value of $10^3\,\mathrm{cm}^{-3}$ to as high as $10^{10}\,\mathrm{cm}^{-3}$ the temperature stays near 10 K. The only exception is for molecular cloud material in the vicinity of newly formed stars, where heating to 30 K or even higher is possible.

Let Γ be the rate of energy gain and Λ the rate of energy loss, both per unit volume. Then, if $\Lambda > \Gamma$ the cooling time scale is given by

$$t_c = \frac{3R_g T\rho}{2\mu(\Lambda - \Gamma)}. \tag{2.34}$$

The basic assumption is that cooling times and heating times are short enough so that an equilibrium is reached, with cooling rate balancing heating rate in determining an equilibrium temperature. A wide range of physical processes is considered to determine the rates [73, 134, 187, 189, 476, 481]; we summarize the important ones here.

The dominant external heating processes are: (1) the photodissociation of molecular H by interstellar photons, (2) the photoionization of carbon atoms by interstellar radiation, (3) the ionization of H and of H_2 by low-energy cosmic rays, and (4) the production of photoelectrons liberated from grains by interstellar UV photons. In these heating processes, the extra energy delivered by the photon or energetic particle, above the ionization or dissociation energy, goes into heating the gas. The heating from these external sources is proportional to the first power of the local gas density. At relatively high densities, above $10^3\,\mathrm{cm}^{-3}$, where most of the gas is in molecular form, cosmic ray heating dominates. The main constituent of cosmic rays is high-energy protons. The heating rate [481] is approximately

$$\Gamma_{CR} = 1.1 \times 10^{-11} \zeta\, n_{H2} \approx 3 \times 10^{-28} n_{H2}\,\mathrm{erg\,cm^{-3}\,s^{-1}}, \tag{2.35}$$

where ζ is the rate of ionization (molecules s^{-1}) of H_2 by cosmic rays, estimated to have a value of $\approx 3 \times 10^{-17}$. This rate actually must be corrected for absorption of cosmic rays in the outer parts of the molecular region.

At still higher densities, where the mass exceeds the local Jeans mass and collapse starts, a fifth process, compressional heating, becomes important. It can be calculated under the assumption that the gas is collapsing at half the free-fall rate:

$$\Gamma_f = -P\rho\frac{dV'}{dt} = \frac{P}{\rho}\frac{d\rho}{dt} = (8G\rho)^{1/2}\frac{R_g T\rho}{(3\pi)^{1/2}\mu} = 2 \times 10^4 \rho^{3/2} T/\mu\,\mathrm{erg\,cm^{-3}\,s^{-1}} \tag{2.36}$$

where Γ_f is the rate of work done by gravity per unit volume, and $V' = 1/\rho$. This approximate relation is obtained by setting dt equal to twice the free-fall time (1.1) and $d\rho/\rho$ to unity, and by using the ideal gas equation for P.

The dominant cooling processes are (1) collisional excitation of atoms, molecules, and ions, by electrons, H, or H_2, followed by radiative decay and escape of the photon, and (2) grain cooling. The cooling rates are all proportional to the square of the particle density. For collisional excitation, the important contributors are C^+ at low densities and C, O, and CO at higher densities; the details of the cooling rates are given in [481]. Grain cooling involves collision of molecules with grains, heating them somewhat but also cooling the gas. The grains then radiate their excess energy in the infrared; they are assumed to behave as miniature black bodies, radiating a Planck spectrum at the grain temperature T_g. As long as the cloud has $\rho < 10^{-13}\,\mathrm{g\,cm^{-3}}$, it is optically thin to this radiation, and it escapes. A molecule arrives on a grain with a temperature T and leaves with the (lower) T_g. The rate of transfer of energy from gas to dust grains is then given by the collision rate per unit volume times the energy loss per collision:

$$\Lambda_g = n_g n_{H_2} v_{H2} \pi r_g^2 k_B (T - T_g) = 3.2 \times 10^{13} \rho_{H2}^2 T^{1/2} (T - T_g) \ \mathrm{erg\,cm^{-3}\,s^{-1}}, \tag{2.37}$$

where the n's are number densities, v_{H2} is the mean of the magnitude (in 3 dimensions) of the velocity of an H_2 molecule $[8k_B T/(\pi m)]^{1/2}$, and r_g, the grain radius, is assumed to be 2×10^{-5} cm. The sticking coefficient is assumed to be 1 and the number density of grains is assumed to be 2×10^{-13} that of H_2. The grain temperature is then determined by the condition that the heating rate of the grain by the above process is equal to the cooling rate by emission of infrared radiation. The emission coefficient is then assumed to be given by $j_\nu = \kappa_\nu B_\nu(T)$, so that $j = 2.3 \times 10^{-4} \kappa_p T_g^4 \ \mathrm{erg\,g^{-1}\,s^{-1}}$ where κ_p is the Planck mean opacity (5.13). The emission coefficient is the energy emitted per unit mass per unit time per unit solid angle per unit frequency interval, so $j\rho$, which is integrated over frequency and solid angle, is the energy emitted by the grains per unit volume per unit time.

To obtain the temperature one makes the assumption that at equilibrium the total rate of heating equals the total rate of cooling:

$$\Gamma_{CR} + \Gamma_f + \Gamma_{\mathrm{photo}} = \Lambda_{ion} + \Lambda_{atomic} + \Lambda_g + \Lambda_{molec} \tag{2.38}$$

where Γ_{photo} is the heating rate from the sum of all processes involving photons, and Λ_{ion}, Λ_{atomic}, and Λ_{molec} refer to collisional excitation processes. Then one solves this expression together with $j\rho = \Lambda_g$ to find T and T_g. It turns out that at lower densities, typical of HI clouds, collisional excitation of C^+ and photoheating are, respectively, the dominant cooling and heating processes, while at molecular cloud densities cosmic ray ionization dominates the heating while CO as well as grains provide the cooling.

Results of heating–cooling balance, based on a particular model of a molecular cloud and under the assumption that $\zeta = 10^{-17}$ [134] show that $T = 70$ K at $n = 35$,

T = 21 K at $n = 4 \times 10^3$, and T = 10 K at density $n = 10^4$ cm^{-3}. Further calculations [300] show that at still higher densities ($\approx 10^6$ cm^{-3}) the gas cools further to 5 K. Nevertheless, the equilibrium temperature varies only slowly for $10^4 < n < 10^{10}$, or $4 \times 10^{-20} < \rho < 4 \times 10^{-14}$ g cm^{-3}. Thus the gas is often assumed to be isothermal at 10 K in that density range. The gas tends to cool on compression, because the heating rate per unit volume is proportional to particle density (also the extinction increases with density), while the cooling rate per unit volume, dominated by collisions, increases with the square of the density. The grain temperature does indeed turn out to be less than the gas temperature and nearly constant as a function of density at about 10 K. At the higher densities, above 10^6 cm^{-3}, the dust and gas temperatures are practically equal at about 5 K.

2.4 Magnetic Braking

The first stage of the solution of the angular momentum problem is to explain why the small-scale, high density regions of molecular clouds have specific angular momentum considerably less than that of the larger-scale regions. One way to solve the problem is to imagine that the turbulent properties of the cores determine their angular momentum [95]. A turbulent velocity distribution consistent with Larson's first finding can be shown to match the observations of angular momentum. The line-of-sight component (v) of the velocity field can be interpreted as rotation, as it shows a velocity gradient across the cloud. Roughly, the specific angular momentum $j \propto vR$ and $v \propto R^{1/2}$ so $j \propto R^{3/2}$, a relation that closely fits the observations (Fig. 2.7). The turbulent velocity field also gives $\beta \approx 0.03$, independent of the size of the cloud, also in agreement with the data in Fig. 2.7. It turns out that the turbulent motions do in fact give an overall net angular momentum to the cloud as a whole.

Another approach, for example in the situation where turbulent effects are not important, is to assume that the high-density regions are connected by magnetic field lines to the lower-density material. Suppose a high-density core has a uniform magnetic field passing through it, and it is rotating faster than the background medium of lower density. If the magnetic field is coupled to both regions, then the field lines will become twisted as a result of the rotation. The equations of magnetohydrodynamics (MHD) show that the twist generates a torque, which slows down the rotation of the high-density material and transfers its angular momentum to the low-density material. The braking of the rotation will continue as long as the time scale for transport of angular momentum is shorter than the contraction time of the high-density region (as the contraction would tend to spin it up).

The braking time was developed in a heuristic manner [151]; more detailed numerical solutions of the equations of MHD have shown that this (highly idealized) argument, summarized in the following paragraph, gives the correct time scale for braking of the cloud.

Consider a spherical cloud with radius R, density ρ, and mass M, threaded by a uniform magnetic field B; an ordered field is required. The cloud is surrounded by external material with lower density ρ_{ext}, which is also threaded by the field. The field is frozen into the gas in both media. The cloud is rotating with uniform angular velocity Ω, parallel to the direction of B, and the external medium is initially not rotating. The field lines become twisted because of the discontinuity in Ω, and the twist propagates outward along the field lines at the Alfvén velocity $V_A = B/(4\pi\rho_{ext})^{1/2}$ (in the external medium). Suppose the initial field is in the Z-direction in a cylindrical coordinate system. Then the twist in the field lines will generate components of the field in the R and ϕ-directions. The torque on an element of material in the cylinder that contains the cloud is then derived from the ϕ-component of the Lorentz force

$$\frac{1}{4\pi}[(\nabla \times \mathbf{B}) \times \mathbf{B}]_\phi .$$

But in the argument, a detailed calculation of the torque is bypassed, and it is simply assumed that the wave spins up the external material within a cylinder with the same radius as that of the cloud until it corotates with the cloud. The angular momentum of the cloud itself decreases correspondingly.

The amount of material accelerated per second in the external medium in a cylindrical shell of radius R and thickness dR as the Alfvén wave passes through it is $2\pi\rho_{ext} R V_A dR$ g s^{-1}. Multiply by the specific angular momentum ΩR^2 to get the angular momentum increase per second for the mass element: $2\pi\rho_{ext} R V_A \Omega R^2 dR$. We assume that the moment of inertia of the sphere $I = 0.4MR^2$ and that its angular momentum is J. We equate the angular momentum loss of the sphere to the angular momentum gain of the external medium, and we integrate over the cylindrical region of external matter through which the Alfvén waves propagate:

$$\frac{dJ}{dt} = 0.4MR^2 \frac{d\Omega}{dt} = -\left(\frac{dJ}{dt}\right)_{ext} = -\pi\rho_{ext} V_A R^4 \Omega \tag{2.39}$$

where the cloud radius is assumed to be constant and where a factor 2 has been introduced to account for wave propagation in both directions.

The braking time is then given by

$$t_b = \frac{\Omega}{\frac{d\Omega}{dt}} = \frac{0.4MR^2}{\pi\rho_{ext} V_A R^4} = \frac{0.4\Sigma}{\rho_{ext} V_A} = \frac{4M}{5(\pi\rho_{ext})^{1/2} BR^2} \approx \frac{0.5\rho}{\rho_{ext}} \frac{R}{V_A} \tag{2.40}$$

where $\Sigma = M/(\pi R^2)$, the surface density of the cloud, and ρ is the density of the cloud. The braking time is thus closely related to the propagation time of the Alfvén

wave into the external medium. The time can be re-written in terms of the critical magnetic Jeans mass: $M_\phi = (BR^2)/(3.6G)^{1/2}$,

$$\frac{M}{BR^2} = (3.6G)^{-1/2}\frac{M}{M_\phi}. \tag{2.41}$$

Then using the free-fall time of the cloud, $t_{\rm ff} = [3\pi/(32G\rho)]^{1/2}$ we obtain

$$t_b \approx 0.4\frac{M}{M_\phi}(\rho/\rho_{ext})^{0.5}t_{\rm ff}. \tag{2.42}$$

For $M/M_\phi \approx 1$, the marginally critical case, the braking time is comparable to the free fall time [357]. For example, if the cloud has $\rho = 10^{-21}\,{\rm g\,cm^{-3}}$ and the density ratio is 10, then we have $t_{\rm ff} = 2\times10^6$ yr and t_b about the same for $M/M_\phi \approx 1$. If the cloud is magnetically subcritical the braking is very fast. Then

$$\Omega_{cloud}(t) = \Omega(0)\ \exp(-t/t_b). \tag{2.43}$$

But if the cloud is supercritical and is already collapsing, a detailed calculation is required to determine how much angular momentum loss occurs. In the limit where the collapse velocity exceeds the Alfvén velocity, magnetic braking is not effective and the cloud collapses with approximate conservation of angular momentum. Also, when the density of the collapsing cloud becomes quite high, the degree of ionization becomes so low that the assumption of complete coupling between matter and field breaks down (Sect. 2.5).

Figure 2.10 shows the results of an analytical solution of the MHD equations for the case of a uniform-density cylinder with radius R and half-height Z_1, linked to the external medium by a uniform field $\mathbf{B}$ along the Z direction [372]. The braking time can be understood as the time required for the Alfvén wave in the external medium to sweep across enough material so that its moment of inertia equals that of the cloud. The figure shows the results for the cloud's $\Omega(t)$ in units of its initial value, assuming it is always uniformly rotating, and that the external medium is initially at rest. The e-folding time for decrease in Ω is found to be

$$t_b = \frac{Z_1}{V_A} \tag{2.44}$$

where Z_1 is the initial half-height of the cylinder, when $\rho = \rho_{\rm ext}$. As the cylinder contracts in Z at constant R, the braking time is independent of the stage of contraction indicated by $\rho/\rho_{\rm ext}$. As an example take a typical molecular clump with $R = Z_1 = 2$ pc and a density of $10^3\,{\rm cm^{-3}}$. If the mean particle mass is 2.3 atomic mass units, then $\rho = 3.8\times10^{-21}\,{\rm g\,cm^{-3}}$ and the total mass is $2.8\times10^3\,{\rm M_\odot}$. Assume that initially $\rho = \rho_{\rm ext}$. Take a field of 30 μG, which gives $M_\phi = 1.2\times10^3\,{\rm M_\odot}$ and

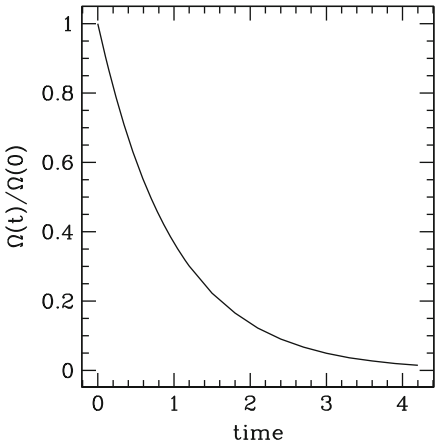

Fig. 2.10 Magnetic braking. The angular velocity of a rotating cloud, in units of its initial value, is plotted as a function of time. The configuration is a uniform-density, uniformly rotating cylinder. The unit of time is the Alfvén wave crossing time Z_1/V_A, where Z_1 is half of the height of the cylindrical cloud at its initial state, when $\rho = \rho_{\rm ext}$, and V_A is the Alfvén velocity in the external medium. Result from [372]

$t_b = 4.5 \times 10^{13}$ sec, only slightly longer than the free-fall time of 3.4×10^{13} s. This assumed cloud is unstable to collapse, and as the density increases, the free-fall time decreases but the braking time remains the same, so eventually the braking becomes ineffective.

In the case where the field and the angular momentum are perpendicular, a similar estimate [371] gives a braking time that is much shorter, up to a factor 10, than in the parallel case. Both of these times are confirmed by detailed complete numerical simulations of the MHD equations [35, 139]. However it is quite possible that the assumed geometry, a uniform parallel or perpendicular magnetic field, is not quite appropriate, particularly when the cloud has contracted to relatively high density. In the case where the magnetic field lines are assumed to diverge spherically from the boundary of the (contracted) cloud, the ratio of braking times between the cases where the angular momentum (**J**) is parallel to **B** to that where **J** is perpendicular to **B** is only about a factor 2 [361]. In this case again the times, assuming the mass-to-flux ratio is close to the critical value, are close to the free-fall time of the cloud. In summary, in the case where a rotating cloud is initially subcritical, its angular velocity will go through three stages. First, the angular velocity will decrease rapidly as a consequence of braking. Second, the angular velocity will remain constant at the background value, as there is no longer any torque on the cloud. Third, when the cloud starts to collapse, the angular velocity will increase again, with approximate conservation of angular momentum, as its collapse time becomes shorter than the braking time.

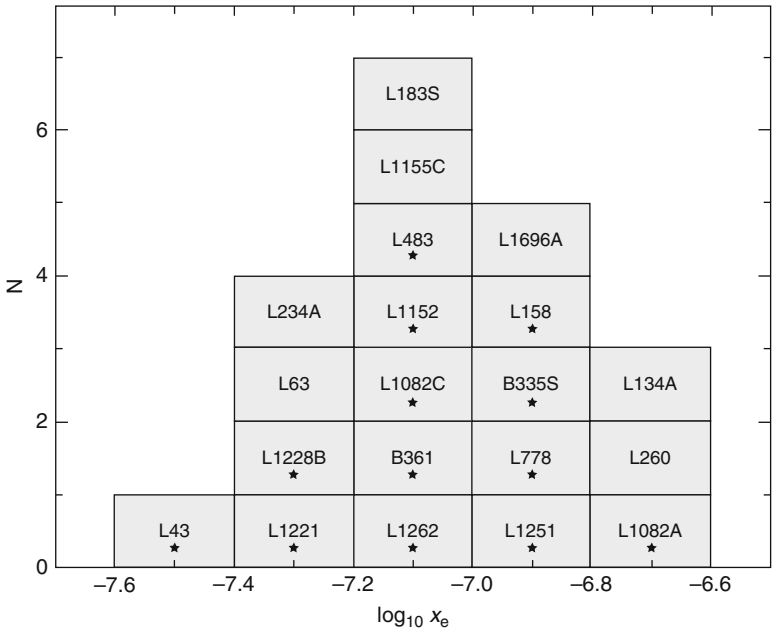

Fig. 2.11 Ionization in molecular cloud cores. The histogram shows the number of cores as a function of the ratio x_e of charged particles to neutral particles. The numbers in the boxes give identifications of the cores observed. A star in a box means that the core has at least one embedded infrared source. Reproduced by permission of the AAS from [551]. © 1998 The American Astronomical Society

2.5 Degree of Ionization

The discussion of magnetic braking assumed that the magnetic field was firmly coupled to the matter, or in other words, magnetic flux was conserved. Coupling requires the presence of charged particles, as well as a sufficient rate of collisions between charged particles and neutral particles such that the neutrals are coupled to the charged particles and therefore are coupled to the field. Define the degree of ionization $x = n_i/n_n$ to be the ratio of the number densities of ionized (positively charged) and neutral particles. In the outer parts of clouds this ratio is determined by photoionization by UV photons from external hot stars. At core densities ($n_n \approx 10^4\,\mathrm{cm}^{-3}$) the UV is attenuated and cosmic ray ionization dominates. It is difficult to measure x in molecular clouds, but a value of 10^{-7} is inferred from observations of the ion HCO^+, which is expected to be one of the dominant charged particles. A set of observations [551] of 20 low-mass cores (mean density $2.5 \times 10^4\,\mathrm{cm}^{-3}$) shows a peak at the above value (Fig. 2.11).

Theoretical work [156] assumes that, at a given density, the cosmic ray ionization is balanced by 2-body recombination of charged particles and recombinations on charged grains, so that a steady-state value of x can be determined. The cosmic

ray ionization rate is ζ per particle per second. In the simplest case of balance, one would have $\zeta n_{H_2} = \alpha_R \times n_i^2$ where the left and right-hand sides, respectively, are the ionization rate and the recombination rate per unit volume, and α_R is the recombination coefficient. So one would have $n_i \propto n_{H_2}^{0.5}$ or

$$x = K_i n_{H_2}^{-0.5} \tag{2.45}$$

where $K_i = (\zeta/\alpha_R)^{1/2} \approx 10^{-5}\,\mathrm{cm}^{-3/2}$, although actually it is a weak function of temperature and density. The degree of ionization is then 10^{-7} at a density of $10^4\,\mathrm{cm}^{-3}$. It has been shown [357] that the $n^{-0.5}$ proportionality is applicable for densities as low as $10^3\,\mathrm{cm}^{-3}$, below which photoionization effects rather than cosmic rays begin to dominate, and the field is effectively coupled. At very high densities, $>10^8\,\mathrm{cm}^{-3}$, the formula is not applicable because cosmic ray ionization effectively shuts off. Some ionization can be provided under these conditions by natural radioactivity. The observations shown in Fig. 2.11 actually are consistent with (2.45) if $K_i \approx 1.4 \times 10^{-5}$, $\zeta = 5 \times 10^{-17}\,\mathrm{s}^{-1}$, and $\alpha_R = 2.5 \times 10^{-7}\,\mathrm{cm}^3\,\mathrm{s}^{-1}$. These quantities are uncertain by at least a factor 2, and the values quoted are within the acceptable range [131, 503]. The recombination coefficient depends on complicated chemistry within molecular clouds and on which particular molecular ion dominates in the recombination process. Thus the relation shown in (2.45) is oversimplified, but nevertheless useful.

2.6 Magnetic Diffusion

In clouds which are not massive enough to contract across magnetic field lines, star formation can occur only if the ratio of mass to magnetic flux is increased. An important process that is considered in this regard is "plasma drift", or "ambipolar diffusion." This effect can be significant at relatively high densities where the degree of ionization is very low and ideal MHD begins to break down. Even if a cloud is magnetically supercritical, but the magnetic field is of some importance, this process will act to reduce the magnetic field effects as the cloud contracts and so contribute to the solution of the "magnetic flux" problem. The process in effect represents the onset of decoupling between the neutral particles and the magnetic field.

Consider a cloud which is in equilibrium with magnetic forces balancing gravitational forces. Neglect pressure forces and assume the cloud is a sphere with radius R, threaded by a uniform field B. Then a rough estimate of the diffusion time, that is, the time required for the neutral particles to drift significantly with respect to the ionized particles, can be derived as follows (from [476]).

The neutral particles are unaffected by the field and tend to drift inward. The ions feel the magnetic force, which is transmitted to the neutrals by collisions. For the neutrals, the force of gravity per unit volume is balanced by the frictional force on

the neutrals by collisions with ions, which in turn is given by the collision rate times the momentum exchange per collision:

$$\frac{GM\rho}{R^2} = n_i \langle \sigma v \rangle n_{H_2} m_{H_2} u_D \ . \tag{2.46}$$

Here v is the actual velocity of the particles, assumed to be $\sim 10^5\,\mathrm{cm\,s^{-1}}$, $\sigma \approx 10^{-14}\,\mathrm{cm^2}$ is the cross section for collision, $\rho = m_{H_2} n_{H_2}$ is the total density of the molecular gas, u_D is the drift velocity of ions relative to neutrals, n_i is the number density of ions, and M is the mass of the cloud. The ions, whose motion is controlled by the magnetic force, satisfy a similar equation, except that the left hand side is replaced by the magnetic force per unit volume, $(\nabla \times B) \times B/(4\pi) \approx B^2/(8\pi R)$. Solving the above equation for u_D, one obtains

$$u_D = \frac{4\pi}{3} \frac{G\rho R}{n_i \langle \sigma v \rangle} \approx R(\frac{10^{-8}}{x}) \ \mathrm{km\,s^{-1}} \tag{2.47}$$

where R is given in parsecs and x is the degree of ionization, n_i/n_{H2}, which is assumed to be small. The time scale for drift out of the core of the cloud is then given by

$$t_{AD} = \frac{R}{u_D} = 5 \times 10^5 (\frac{x}{10^{-8}}) \ \mathrm{yr}. \tag{2.48}$$

Even if x is as small as 10^{-5}, the time scale is long, about 5×10^8 yr. At a number density of 10^6, the degree of ionization (2.45) is small enough (10^{-8}) for the time scale to come down to 5×10^5 yr. But this result shows that in most of the mass of molecular clouds, which has much lower densities, ambipolar diffusion is not important on reasonable time scales. However if turbulence is present and there are local strong compressions of the material, the ambipolar diffusion time is speeded up by a factor of a few [384].

Going back to (2.47), we find that the diffusion time is given by

$$t_{AD} = \frac{x n_n \langle \sigma v \rangle}{4/3\pi G \rho_n} = \frac{3 K_i n_{H_2}^{0.5} \langle \sigma v \rangle}{4\pi G m_{H_2} n_{H_2}} \tag{2.49}$$

and

$$\frac{t_{AD}}{t_{ff}} = \frac{3 K_i \langle \sigma v \rangle}{4\pi G^{1/2} m_{H_2}^{0.5} (3\pi/32)^{0.5}} = 19. \tag{2.50}$$

The numerical value depends on the composition, the cloud geometry, and K_i but in any case it is of order 10. This relation is very important because it implies that subcritical non-turbulent molecular clumps, which are supported by the magnetic field, evolve quasistatically. Note that the above ratio depends both on the assumption of equilibrium and on the validity of the ionization law. Although the value of the field B does not appear in the above expression, it is implicitly present through the assumption of equilibrium. To see how the result depends on B, just

replace the left-hand side of (2.46) by $B^2/(8\pi R)$ (follows from equating magnetic energy to gravitational energy GM^2/R), solve as before for u_D and t_{AD}, and set $K_i = 1.4 \times 10^{-5}$ to obtain

$$t_{AD} \approx 4 \times 10^6 \text{ yr} \left(\frac{n_{\text{H2}}}{10^4 \text{ cm}^{-3}}\right)^{3/2} \left(\frac{B}{30\mu G}\right)^{-2} \left(\frac{R}{0.1 \text{ pc}}\right)^2. \tag{2.51}$$

The times given by (2.48) and (2.51) are in good agreement with more detailed numerical modelling of equilibrium cloud structures, including ambipolar diffusion, supported against gravity by magnetic fields and pressure effects [325, 386, 507], as well as with calculations that extend into the early part of the collapse phase [35, 171]. During the quasistatic phase the central value of the field evolves approximately as $B_c \propto n_c^{0.5}$. When the central densities increase to the range 10^5–10^6 cm^{-3}, sufficient diffusion has taken place so that the central regions become unstable to gravitational collapse. At this point the magnetic field is still present, and it is still coupled to some extent to the gas even though the degree of ionization is very low. However it is no longer dynamically important; a relatively small flux loss (factor 2) goes a long way in allowing the central regions to go supercritical, partly because of flow along field lines.

Some other conclusions from such calculations are as follows: (1) Ambipolar diffusion can produce cloud cores but the process requires 10 initial free-fall times, so if one starts from $n_{\text{H2}} = 10^3$ cm^{-3}, long time scales ($\approx 10^7$ yr) are required. Only moderate flux loss is required. Therefore the magnetic flux problem remains to be solved at higher densities. (2) This long time scale is definitely a problem, since practically all (90%) molecular clouds in the Galaxy show some evidence of star formation. Supersonic turbulence might help, compressing the magnetic field in shocked regions and reducing t_{AD} in some regions. Also, analytical and numerical calculations show [115] that if the cloud is approximated as a thin disk, t_{AD} can be considerably reduced from 10 t_{ff} if the initial mass-to-flux ratio is close to the critical value. (3) Once the cloud core has been formed, runaway collapse can occur at the center after $\sim 2 \times 10^5$ yr. The radial density distribution in the core as it begins collapse is close to $\rho \propto R^{-2}$. (4) Observed core shapes are not good indicators of physical conditions, that is, directions of angular momentum and magnetic field. A flattened cloud core does not necessarily mean that the angular momentum or magnetic field vectors lie along the short axis. (5) The diffusion times derived above assumed equilibrium between magnetic and gravitational forces, that is $M \approx M_\phi$. If, as observed, some regions are already supercritical, they could evolve quickly to the core stage, limited by the decay time of turbulence. Thus the diffusion model does allow star formation over a range of time scales (slow star formation) and could be consistent with the range of ages in a young cluster, such as NGC 2264.

Nevertheless some criticisms of the ambipolar-diffusion picture remain. (1) Observations of magnetic fields suggest that most clumps and cores, over a range of densities, are already supercritical, so diffusion isn't needed. Even though there are observational uncertainties in magnetic field observations, there are enough

clumps and cores with unobserved or low fields to account for the rate of star formation. (2) If ambipolar diffusion were the dominant process controlling star formation, there would be many more high-density cores in molecular clouds without embedded infrared sources (starless cores) than cores with embedded protostellar objects, because the time scale for the protostellar phase is only about $2 - 3 \times 10^5$ years. A starless core is defined as one which is gravitationally bound and therefore likely to eventually become a protostar, but which has no detectable evidence for an embedded protostar. Surveys have been made of the numbers of starless cores versus cores containing protostars over various star-forming regions [442]. The ratio is found to be about 3 to 1, but different studies have given different results. Thus the lifetime of a starless core, at a density close to $10^5\,\mathrm{cm}^{-3}$ is $\approx 6 \times 10^5$ yr. The free-fall time in the density range of the observed cores is $1 - 2 \times 10^5$ yr. The lifetime is definitely shorter than one would expect from the ambipolar diffusion model; on the other hand it is longer than the lifetime of a core that one would expect in a supersonically turbulent model (next section), which is only 1–2 free-fall times. This kind of study has been done for various density ranges [537], with the same result. The lifetime of a core is always a few free-fall times, but definitely less than 10. If true, the implication is that cores, once formed, do not immediately go into dynamical collapse, but they do evolve on a time scale shorter than that of ambipolar diffusion.

2.7 How is Star Formation Initiated?

Three different scenarios are being discussed regarding the process by which a cloud core is brought to the onset of collapse:

1. Low-mass cores are assumed to be magnetically subcritical, that is magnetic effects prevent collapse and support molecular clouds. The densest regions evolve to the onset of collapse, controlled by ambipolar diffusion (slow drift of neutral particles across magnetic field lines). The time scale is a few million to 10^7 yr.
2. Star formation is controlled by turbulence. Supersonic turbulence generates a complicated shock pattern. Randomly produced shock-compressed regions of high density can occasionally reach the point of instability to collapse. The time scale is much shorter, more like 10^6 yr, and the efficiency of star formation is tied to the properties of the underlying turbulence.
3. Cores that are intrinsically stable to collapse are forced into collapse by a specific event, an external trigger such as an ionization front, a supernova shock wave, or a cloud–cloud collision. The time scale then is the shock crossing time, which could be as short as 10^5 yr.

The first of these possibilities was discussed in the previous section. Existing observations of magnetic fields in the precursors of cloud cores indicate that most of them, but not all, are supercritical. Even when they are supercritical, the magnetic

field is still of some importance and cannot be left out of a theory of star formation. For example, in supercritical regions, ambipolar diffusion will still take place, but it is not necessary for the initiation of star formation. It is likely that all three of the possibilities just mentioned play some role in the theory. Nevertheless, more emphasis is now being placed on the second and third alternatives, which are discussed in the next two sections.

2.8 Turbulence and Star Formation

The study of turbulence in the laboratory involves relatively incompressible fluids and subsonic velocities. The general criterion for onset of turbulence is a Reynolds number ($R_e = vL/\nu$, where v is a typical velocity, L is a typical length, and ν is the molecular viscosity) greater than a critical value, which differs for different situations but is typically several thousand. Once turbulence develops, motions develop on a wide range of scales. The general picture is that energy is fed into the turbulence on the largest scale, and it is transmitted through the so-called "turbulent cascade" to smaller and smaller scales, until it reaches a very small scale on which it is dissipated into heat. The relation between typical velocity and length scale is known as Kolmogorov's law, in which $v \propto L^{1/3}$. Thus most of the kinetic energy is on the large scales. The dissipation scale is given roughly by

$$\frac{L_{\rm diss}}{L_m} = R_e^{-3/4} \tag{2.52}$$

where L_m is the scale of energy input. In molecular clouds the dissipation scale is estimated to be only $\approx 3 \times 10^{-5}$ pc [352]. Reynolds numbers on the molecular cloud scale (Table 2.1) can be estimated using $v \approx 3\,{\rm km\,s^{-1}}$, $L \approx 5$ parsecs, $\nu \approx c_s \lambda_m$ where $\lambda_m = 1/(n\sigma_m)$ is the particle mean free path (about 10^{13} cm), and σ_m is the particle scattering cross section, typically 10^{-15} cm^2 for neutral particles. The result is $R_e \sim 10^7$, well in excess of the critical value for the onset of turbulence.

The origin of interstellar turbulence is unclear [29]. Some theories of the origin include instabilities induced by colliding flows in the interstellar gas [213], magnetorotational instability in galactic disks [417], and instabilities that develop behind the spiral waves in the galaxy [80]. It is clear that the turbulence is compressible, and it is supersonic, on the larger scales, with respect to the cold molecular cloud material. Nevertheless it retains some properties of laboratory turbulence. We have seen, from Larson's first finding, that approximately $v \propto L^{1/2}$; thus most of the kinetic energy is still on large scales. There also is a turbulent cascade, or an approximation to it, but the energy input is not necessarily limited to the largest scales, although these scales for energy input may dominate. Also, the dissipation is not necessarily occurring on the smallest scales, because the random supersonic motions produce shock waves, which can dissipate kinetic energy into heat on various scales. On a given scale, the flow can be characterized by a turbulent Mach number, the ratio of the root-mean-square turbulent velocity (in 3 space

dimensions) to the sound speed. On the molecular clump scale (2 pc) this ratio is of order 10. On the other hand, the flow speed is comparable to the Alfvén speed. Measurements on various scales in molecular clouds indicate rough equipartition between gravitational, magnetic, and turbulent energy; thus the clouds are supported against gravity in the global sense. A detailed discussion of interstellar turbulence appears in [352].

The key to star formation by turbulent effects is the local phenomenon of transient compression of certain regions by shock waves. If the overdense regions behind the shocks are massive enough and long-lived enough, they can become Jeans unstable and begin to collapse. The random nature of the strength of these shock events suggests that star formation is possible but inefficient. Shock wave dissipation also implies that supersonic turbulence, without continuous energy input, must decay on a time scale comparable to that for a strong shock to propagate across the largest eddies, which for a 5 pc scale is $O(10^6)$ yr [186].

Numerical simulations of turbulence, which require 3-dimensional hydrodynamics, can only approximate the actual situation. However such simulations, both with and without magnetic fields [29, 335] verify the qualitative picture described above that the kinetic energy in turbulence, at least on the larger scales, decays. Some of the important points that emerge include: (1) A clumpy structure develops with the maximum fluctuation in density increasing with turbulent Mach number. (2) Turbulence decays, even with the presence of magnetic fields, on a time scale L/v_{rms}, where L is approximately the scale of the system and v_{rms} is the rms velocity of the turbulence. This time scale for a 1 parsec cloud and an rms velocity of 1 km/s again is about 10^6 yr.; it scales as $L^{1/2}$. If this occurred in a cloud of a few hundred solar masses, the cloud after decay would have several hundred thermal Jeans masses, and could form a small cluster. (3) Even if turbulence is maintained by some driving mechanism and it is able to support the cloud overall, locally high-density regions are generated randomly as a result of the turbulence. Some of them could exceed the local Jeans mass for long enough to allow collapse to stars. The resulting star formation efficiency turns out to depend on the driving scale of the turbulence. (4) Some mechanism to maintain the turbulence in the ISM is required, in order to explain the observations that all molecular clouds have line widths above thermal, and to prevent overall collapse of molecular clouds and a star formation rate that is much higher than that observed. If there is no continual energy input, one is driven to the conclusion [203] that the turbulence must have been generated as part of the process by which the molecular cloud was formed, for example by large-scale colliding gas flows. In this scenario star formation would have to occur rather quickly, in less than a crossing time, in a relatively small amount of material that becomes gravitationally bound. Then, on the same time scale as that of the decay of turbulence, the cloud is disrupted by stellar feedback. The conclusion then would be that lifetimes of even the largest clouds are only 2–3 Myr, a result that is being debated.

With regard to point number (2), numerical simulations both with and without magnetic fields show that without external energy input the turbulence does decay on short time scales [334, 494]. Simulations (Fig. 2.12) show that in 0.4 sound

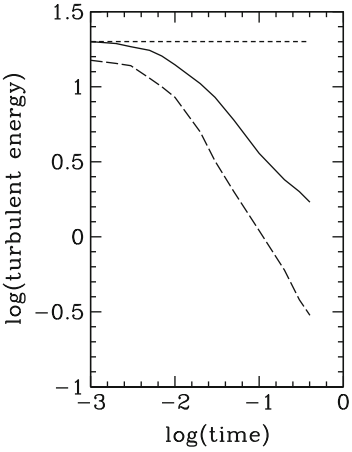

Fig. 2.12 Decay of turbulence in molecular clouds, according to three-dimensional numerical simulations, after [494]. The horizontal axis gives the log of the time in units of the sound crossing time. The vertical axis gives the log of the kinetic energy plus the magnetic energy in turbulent fluctuations, in non-dimensional units. *Short dashed line*: Turbulent energy is continuously supplied to the grid, at a fixed rate, leading to a steady state. *Solid line:* The turbulence is allowed to decay, with no energy input. The initial ratio of gas pressure to magnetic pressure is 0.01, corresponding to a magnetic field far stronger than observed. *Long dashed line:* decay of turbulence with no magnetic field

crossing times, which corresponds to about 2 turbulent crossing times for the calculation shown, the kinetic energy decreases by a factor 10 even if a very strong magnetic field is present. Without the field the decay in the energy is closer to a factor 50. Much of the dissipation occurs in shocks, but some energy is lost by energy cascading to smaller length scales and then being numerically dissipated at the grid scale. The upper curve shows how the energy in turbulence saturates if energy is supplied at a given rate by input of a random velocity field.

An independent calculation [334] yielded similar results. The turbulent energy decayed as approximately t^{-1}, fairly independent of whether or not magnetic fields were present, and the characteristic decay time is about 0.5 of the turbulent crossing time, based on a turbulent Mach number of 5. The calculations are performed with both a smoothed-particle hydrodynamics (SPH) numerical code and a standard fixed-grid code, with very similar results. These simulations support the suggestion [202, 387] that the time scale of star formation is that of turbulent decay rather than ambipolar diffusion, under the further assumption that there is no significant source of driving for the turbulence. However if star formation took place on a time scale of only a million years in molecular clouds, even if the efficiency were only 2%, the rate of star formation in the galaxy would be far higher than observed.

The alternative to pure turbulent decay in molecular clouds is continuous driving of the turbulence by some process that is not well understood (point 4). Some of the possibilities are supernova shocks, outflows from embedded young stars, HII

regions, or galactic rotational shear. Nor is it understood how the energy, if injected on large scales, cascades down to small scales to limit star formation. Conversely, if energy is injected on small scales, as it would be from bipolar flows from newly formed stars, it is difficult to explain the high turbulent velocities observed on large scales. Of course there could be more than one driving mechanism, and the expansion of HII regions is a promising way to do the driving on large scales. Nevertheless if it takes 10 cloud free-fall times to form a significant number of stars, which can occur for reasonable assumptions regarding the scale of the turbulence, and the molecular cloud is blown away on that time scale, it may be possible to explain a low efficiency of star formation. If the driving scale of the turbulence is long, or if it is not driven at all, local collapse will occur, star formation will be efficient, and cluster formation could occur. The alternative, mentioned above is that the turbulence is not driven, but is generated by initial conditions, and that the time scale for star formation is the same as that for turbulent decay, and once the star formation occurs, the molecular cloud is dissipated.

Extensive work has been done to simulate numerically the effects of turbulence on star formation. The typical simulation has a box size of 0.1–1 pc and a mass 100–1,000 $M_\odot$. Thus, assuming that the initial cloud fragments, these simulations represent cluster formation. The main question to be considered here is whether the simulations come up with the same approximate star formation efficiency as is observed. The different simulations include different physical effects, and the point is to determine which of these effects is the most important in determining the star formation efficiency. Such simulations address other questions as well, notably the form of the initial mass function and the properties of the resulting binary and multiple systems; these questions are discussed in other chapters of this book.

Suppose one considers pure hydrodynamic turbulence with no driving, no magnetic fields, and no feedback effects from the stars that have formed. The initial turbulence just decays and the cloud fragments into protostars. SPH calculations [258] were performed for an isothermal gas in a box which originally contained 222 thermal Jeans masses but had turbulent kinetic energy comparable to gravitational energy. Random density fluctuations are introduced to represent the initial turbulence. The simulation included 500,000 particles and is shown in Fig. 2.13. When the gas density in a local region exceeds a given minimum, and the particles in the region are gravitationally bound, the collection of particles is collected into one "sink" particle, that represents an unresolved collapsing protostar. The first box represents the initial condition, and the three remaining boxes represent times at which 10%, 30%, and 60% of the mass has collected into the collapsing protostellar cores (black dots). The resulting clump mass spectrum looks something like $dN/dM \propto M^{-1.5}$ (similar to what is observed in the interstellar medium). The core mass spectrum has a lognormal shape – that is, a Gaussian in log M – peaked at about twice the Jeans mass of the original cloud. The conclusion is that after only 2 free-fall times (final panel) 60% of the mass of the initial cloud has been converted into a small cluster of protostars, an efficiency much larger than observed, for the overall ISM, and larger even than what actually occurs locally in cluster-forming regions (<30 %).

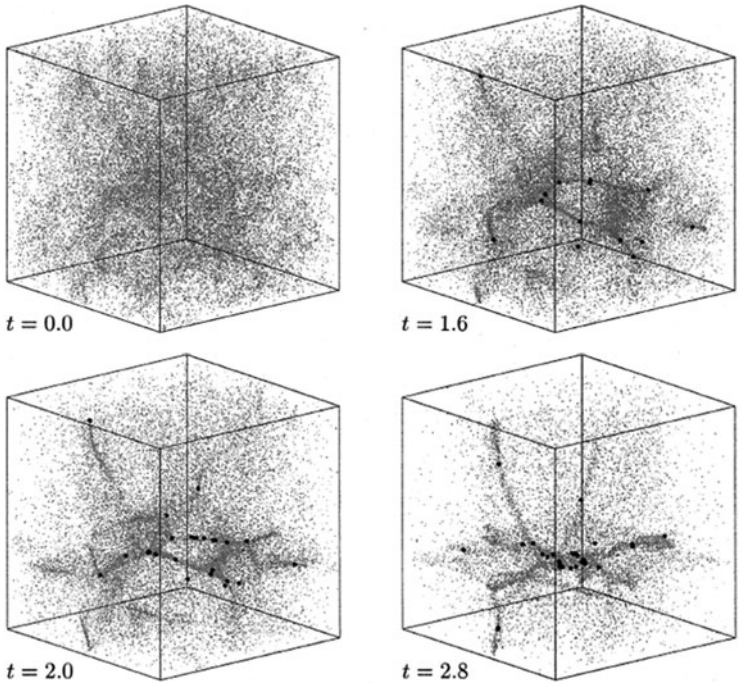

Fig. 2.13 Decay of turbulence in molecular clouds and formation of a protostellar cluster, according to three-dimensional numerical simulations with an SPH code. If the initial density in the cloud is taken to be 10^5 particles cm^{-3} then the size of the box is 0.32 parsec and the unit of time is 6.9×10^4 years. The total number of particles in the simulation is 500,000, not all of which are shown. Reproduced by permission of the AAS from [258].

Further simulations investigate the question of whether driving the turbulence continuously has an effect on reducing the star formation efficiency. Here the overall picture would be that energy is injected at a sufficient rate to match the decay rate, so that the molecular cloud reaches a steady state, supported overall against collapse by the turbulence, and having a lifetime of say 3 crossing times before the onset of disruption by stellar feedback. In one example [259] the velocity fluctuations that are introduced to drive the turbulence have a scale of 1/4 to 1/3 the size of the box. Calculations have been performed with both grid-based and SPH numerical codes. The cloud is globally stable against collapse. The high-density compressed regions randomly produced by shocks in such flows are the sites of local collapse and star formation even if turbulent energy integrated over the cloud is sufficient to support it against gravity. At the end about 50% of the mass of the cloud has been converted to dense collapsing cores, but the time scale (seven initial free-fall times) is about three times longer than in the case of decaying turbulence. Thus even driven turbulence gives fairly efficient star formation, but further simulations

show that the efficiency drops as the driving scale decreases. The only way, in this purely hydrodynamic picture, to prevent star formation altogether (or at least make it very inefficient) is to introduce high Mach number turbulence, so that even on the smaller scales the turbulent energy is greater than gravitational, and also to drive the turbulence on very small scales (say 30 or 40 wavelengths per box) so that the driving wavelength is smaller than the local Jeans length. However the results show that the Mach numbers needed to explain the observed low efficiency are unrealistically high, and the driving scales needed are unrealistically low, so this approach does not necessarily explain the low efficiency of star formation.

Another SPH calculation [79] with turbulent initial conditions but no driving and no feedback includes 500,000 particles and starts with a cloud of 1,000 solar masses and a diameter of 1 parsec. The cloud initially has about 1,000 thermal Jeans masses, but it is supported by a random turbulent velocity field with total turbulent energy equal to the gravitational energy; the corresponding mean line-of-sight turbulent velocity is about 1.3 km/s, approximately Mach 6. The gravity is softened on a scale of 160 AU, which determines the effective resolution, so many binaries are not resolved, nor are disks. The lowest mass that is resolved is about $0.1\,M_\odot$. The calculation proceeds through a dissipation phase which lasts about 1 free-fall time. During the decay of the turbulence it produces filamentary structures and locally high-density regions. These regions form the nucleus of about 5 subclusters, in each of which a few tens of stars fragment out. Figure 2.14 shows the column density through the calculated box of 1 pc on a side. The subclusters begin to merge (panel C) and at the termination of the calculation (2.6 free-fall times) a single centrally condensed cluster of more than 400 stars has formed, with a maximum stellar mass of $27\,M_\odot$. At this time 42% of the initial mass remains in gas, giving a high star formation efficiency. The mass function at the end of the simulation has a slope of about -1.0 at the high-mass end, while the Salpeter slope is -1.3. The turnover at masses below solar is in qualitative agreement with observations. In the subclusters the stellar density is very high, so many (about a third, including most of the high-mass objects) objects have close encounters of 100 AU or less, which would truncate their disks, and possibly harden binary systems and disrupt planetary systems. Again, this calculation has been criticized on the grounds that, had the simulation been carried to longer times, the star formation efficiency would be far larger than observed.

A calculation with similar physical assumptions but much higher numerical resolution [37] starts with a cloud of $500\,M_\odot$, temperature 10 K, and size 0.4 pc. The calculation provides very detailed results on the properties of the IMF and of the stellar multiple systems (Chap. 6). However, after only 1.5 initial free-fall times the stars and brown dwarfs contain 191 $M_\odot$. Had the calculation been continued it would again have produced a high star-formation efficiency.

A hydrodynamics simulation with additional effects [319, 385], was performed on a 128^3 grid, with a magnetic field (treated as ideal MHD) included, and with feedback effects resulting from the assumed bipolar outflows generated by the forming stars. The cloud is supercritical, with mass to flux ratio about 2 times the critical value. The initial turbulence decays, and is not driven externally, but

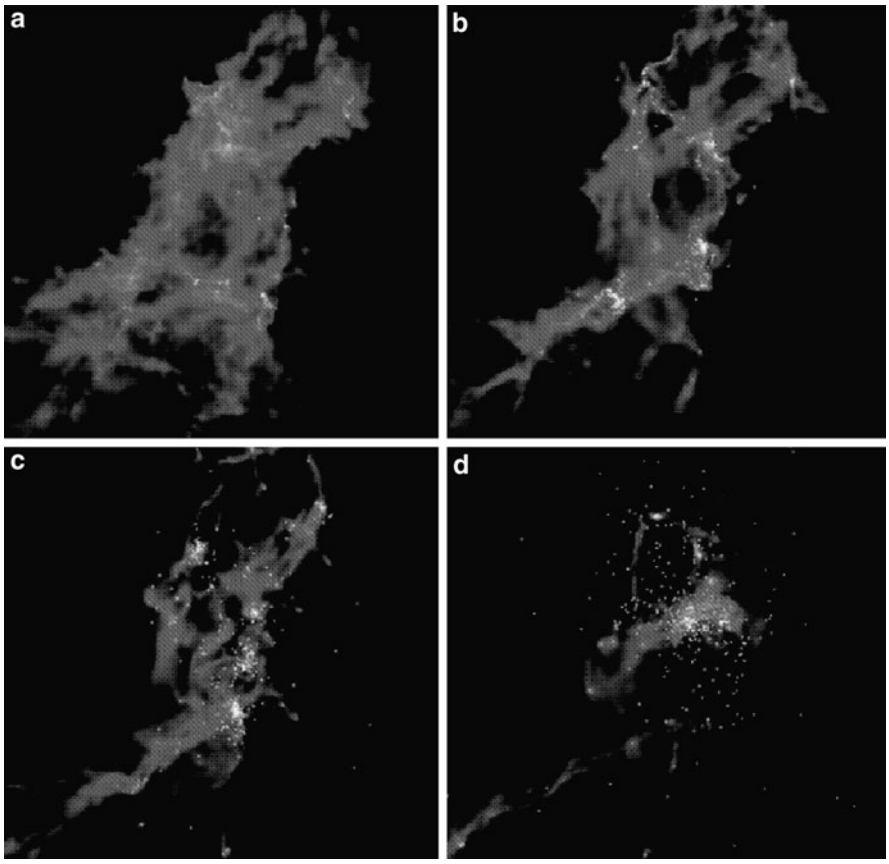

Fig. 2.14 Formation of a stellar cluster from a turbulent molecular cloud region. The grey scale indicates the log of the column density, ranging from $0.025\,\mathrm{g\,cm^{-2}}$ (*dark*) to $250\,\mathrm{g\,cm^{-2}}$ (*light*) [79]. The *light dots* indicate stars. The frames are 1 pc on a side. The evolution of the system of $1{,}000\,\mathrm{M_\odot}$ is plotted at times of 1.0 (**a**), 1.4 (**b**), 1.8 (**c**) , and 2.4 (**d**), in units of the initial free-fall time of 1.9×10^5 yr. Reproduced by permission of John Wiley and Sons Ltd. from I. A. Bonnell, M. R. Bate, S. G. Vine: *MNRAS* **343**, 413 (2003).

once stars form, it is assumed that they generate bipolar outflows, with momentum proportional to the current stellar mass and with a typical velocity of about $50\,\mathrm{km\,s^{-1}}$. The injection of momentum re-energizes the turbulence from within, and with the parameters chosen, the cluster-forming cloud remains in near virial equilibrium, and the formation of subsequent stars is delayed. In the standard simulation, the cloud had a radius of about 1.5 pc and a mass of $\sim 1{,}000\,\mathrm{M_\odot}$. After 2 initial free-fall times, or roughly 1 Myr, the star-formation efficiency was only 3%. The model contains a number of arbitrary but reasonable parameters, and as one would expect, as the strength of the outflow (as measured by the outflow momentum per unit stellar mass) decreases, the efficiency increases, in inverse

proportion. The effect of increasing the magnetic field is to reduce the efficiency. If the magnetic field is reduced to a negligible value, the efficiency increases by a factor of ≈ 2 relative to the standard case.

A further physical effect that must be considered is the feedback on the collapsing cloud resulting from the luminosity of the protostars that have formed within it. In numerical simulations, first, the luminosities, which are derived mainly from accretion, must be estimated, and second, the transfer of this radiation outward through the cloud must be calculated. In the previous calculations discussed above, radiative transfer was not considered, but simple approximations for the temperature of the gas were used (Chap. 3). The addition of this effect to three-dimensional numerical codes results in a significant enhancement of required computing time, so the simulations cannot be followed as far as those with simpler physics. An initial calculation of this type [38] shows that in a cloud of $50\,\mathrm{M}_\odot$ after 1.4 initial free-fall times the number of stars formed is reduced by a factor 2 compared to the calculation without radiative transfer, and the number of brown dwarfs is reduced by a factor of about 5. However the total mass of stars and brown dwarfs formed is not significantly changed. A further simulation [424], with the same cloud mass and including magnetic fields, shows that the effect of radiation transfer is to reduce the efficiency slightly, and that the combined effects of radiation transfer and an initial magnetic field with a mass to flux ratio 3 times critical (similar to the observed value) gives an efficiency per free-fall time (see below) of about 10%. Without the magnetic field the efficiency is a factor 2–3 higher. However the calculation was carried only about 1.3 initial free-fall times. The physical effect of the magnetic field is to slow down the collapse on large scales and thus to reduce the rate of star formation. Radiative transfer effects do not become important until protostars have formed, and the effect is to heat the surroundings, increasing the Jeans mass and suppressing further star formation locally, on small scales.

How are these numerical results on star formation efficiency to be compared with observations? The answer to this question proves to be difficult when one considers the details. First we consider the various possibilities of defining the efficiency, going beyond the global and very general definition given in (1.4).

For a single molecular cloud core that forms a single stellar system the efficiency is

$$\epsilon_{\mathrm{core}} = \frac{M_*}{M_{\mathrm{core}}} \tag{2.53}$$

where the part of the core that doesn't accrete onto the star within it is assumed to have been ejected by the effects of stellar outflows. In an analytic model of collimated bipolar protostellar outflows [346], the results show an ϵ_{core} of about 25% for spherical cores and about 75% for cores with a high degree of flattening. These results are roughly consistent with observations [15] that show that the initial mass function of cores in a star forming region has the same shape as that for stars, but is displaced upwards by a factor of about 3 (Fig. 2.6). In principle, the radiation from the protostar could also affect the efficiency; this effect turns out to be important for high-mass stars (Chap. 5) but not for low-mass stars.

For a cluster-forming clump, the total efficiency, defined when star formation is complete, is

$$\epsilon_{\rm tot} = \frac{M_*}{M_{\rm clump,init}} \tag{2.54}$$

where M_* is the total mass in stars and $M_{\rm clump,init}$ is the original total mass of the clump. This quantity is difficult to determine observationally, because by the time all the stars have formed, much of the remaining gas has been dissipated. Thus the observed efficiency is based on the current values of star mass and clump mass

$$\epsilon_{\rm clump} = \frac{M_*}{M_* + M_{\rm clump}} \tag{2.55}$$

where $M_{\rm clump}$ is now the current clump mass, not counting that which has already been dissipated. Thus this efficiency is a function of time, with values ranging from zero to one. It is difficult to determine for a given observed cluster what its evolutionary history was and to compare with theory, where the typical calculation is stopped at 1 or 2 initial free-fall times. Observed values of $\epsilon_{\rm clump}$ in embedded clusters, still in the process of formation, range from 8 to 33% [289]. Even smaller values (3 to 6%) are obtained for five nearby star-formation regions based on infrared observations by Spitzer [164]. It is possible that these efficiencies correlate with the age of the system, as expected. The average value is higher than the overall efficiency for a molecular cloud as a whole, where it is estimated to be roughly 2%.

A more meaningful comparison with observations can be obtained through use of still another definition of the efficiency [283]. The dimensionless star formation rate per free-fall time, equivalent to the efficiency per free-fall time, is defined in terms of the density of the object considered:

$$\epsilon_{\rm ff} = SFR_{\rm ff} = \frac{\dot{M}_* t_{\rm ff}(\rho)}{M(>\rho)} \tag{2.56}$$

where $M(>\rho)$ is the mass within a given volume with density greater than a threshhold value ρ, and $t_{\rm ff}(\rho)$ is the free-fall time at that density. The quantities on the right-hand side can be estimated from observations; note that the uncertain molecular cloud lifetime does not enter. For densities varying from 10^2 to 10^5 cm^{-3}, observations show that the quantity $\epsilon_{\rm ff}$ does not vary significantly, and on the average falls in the range 1–3%. By way of comparison, the overall efficiency per free-fall time, averaged over all the molecular clouds in the Galaxy, is about 1%. The numerical simulations involving hydrodynamics with decaying or driven turbulence, which start in the same density range, give much higher values, closer to 20–30% (per free-fall time). In the model with a magnetic field and regeneration of turbulence through outflows [385] the computed efficiency per free-fall time is about 3%. The implication is that clusters form relatively slowly, over many free-fall times. The model with a magnetic field and radiative transfer, although preliminary, gives a value of about 10%.

Although many aspects of the star formation problem still remain unresolved, the introduction of the theory and simulations involving supersonic turbulence have resulted in progress. The observational results over a wide range of scales show that the velocity dispersion scales with the square root of the size of the region; this fact is a strong argument for the existence of supersonic turbulence. Although it is no longer believed that most star formation occurs in magnetically subcritical cores and is controlled by the ambipolar diffusion time, still the magnetic fields must have some influence on the overall process. The magnetic energy in molecular clouds is known to be comparable to the turbulent kinetic energy. Thus the combination of turbulence and magnetic fields in numerical simulations is necessary, although difficult. Eventually, inclusion of even more physical effects in such simulations, along with simultaneous treatment of a wide range of scales, from the size of a whole molecular cloud (parsecs) down to a few solar radii, should result in further progress on this key problem.

2.9 Induced Star Formation

There is some evidence to suggest that star formation may have been induced, not only by turbulent effects, as mentioned in the previous section, but by other kinds of shocks. Induced (or "triggered") star formation simply means that interstellar clouds with masses originally less than their Jeans mass are compressed by some external agent, resulting in a reduction of their Jeans mass to the point where they are forced into collapse. On large scales, galaxy-galaxy mergers as well as galactic spiral arms can induce such compressions. In this section we consider the smaller-scale processes of star formation induced by supernova shock waves, by expanding HII regions, and by cloud–cloud collisions. Although there is some observational evidence that induced star formation has occurred, it is still thought that most star formation occurs by the "spontaneous" processes described in the previous sections.

The supernova shock trigger for star formation is supported by the argument that meteoritic material in the solar system is known [311] to have had live (radioactive) ^{26}Al, which has a half-life of only 0.7 Myr, in it at the time of solidification, as well as a number of other so-called extinct radioactivities [193], including ^{60}Fe, with a half-life of 1.5 Myr. The ^{26}Al decays to ^{26}Mg which is found in meteorites in excess of the normal isotope ratio ^{26}Mg/ ^{24}Mg. Since the ^{26}Al was presumably produced in supernovae, some material in the ejecta must have travelled to a molecular cloud, been injected into a cloud core, evolved to the onset of collapse, collapsed into a disk, and solidified, all in a time of order 1 Myr. Both the magnetic diffusion picture and the turbulent star formation picture would have difficulty explaining this short time scale.

However it is possible that the collapse of molecular cloud material could have been induced on a shorter time scale by the same event that produced the ^{26}Al, namely the supernova shock wave [104]. Numerous calculations, for example [86, 493, 501], have been made of the interaction between clouds and shocks of

various kinds. For example, consider a supernova which is set off with an energy of 10^{51} ergs, 10 parsecs away from a pre-existing relatively dense cloud of radius 1 parsec. The shock hits the cloud at 1,000 km/s. A transmitted shock is sent into the cloud, which moves more slowly than the shock outside the cloud. The main shock wraps around the cloud and meets with itself at the back, sending another shock back into the cloud and also one headed away from the cloud. Effects caused by the shock include acceleration of the cloud, stripping of the outer edge of the cloud, and compression of the interior. The shock that wraps around the outside of the cloud induces Kelvin–Helmholtz and other instabilities which tend to shred the cloud. If the cooling time behind the shock is long compared to the time for the shock to cross the cloud, then the cloud will reexpand after passage of the shock and will not be forced into collapse. If the cooling time is short, there is a chance that star formation can be induced, but it still must happen before the cloud is shredded. In general it seems to be difficult for star formation to be induced by such an event. Nevertheless there is observational evidence supporting this picture: a detailed study of the Upper Scorpius OB association [419] strongly suggests that star formation there was initiated by a supernova shock.

The following argument [157] illustrates in a simple way how to get conditions favorable for shock-induced star formation. Note that the way the Jeans length is written in (2.62) implies that if the cloud $R > R_{\rm Jeans}$ it will be unstable to collapse even before the shock hits it.

To estimate the likelihood, we can compare the gravitational collapse time of the cloud at the post-shock compressed density to the time it takes for the shock to destroy the cloud through Rayleigh–Taylor and related instabilities. The cloud destruction occurs by the interaction of its surface gas with the fast post-shock flow that propagates just outside the cloud. The velocity shear generates the instabilities, and numerical simulations [255, 392] show that the time for the cloud to be torn apart is about 3 times longer than the time for the shock to propagate through the inside of the cloud. The destruction time is

$$t_{\rm dest} \approx \frac{3R}{v_{\rm s}(\rho_0/\rho_{\rm c})^{1/2}} \tag{2.57}$$

where the cloud has initial density $\rho_{\rm c}$ and radius R, and the interstellar gas outside the cloud has density ρ_0. The propagation speed of the shock outside the cloud is $v_{\rm s}$ and that inside the cloud [351] is the denominator on the right-hand side of (2.57), in the limit of a strong shock.

Let $c_{\rm c}$ and $c_{\rm cA}$ represent, respectively, the sound speed in the cloud before and after the shock hits it. Let $\rho_{\rm cA}$ be the compressed density in the cloud behind the shock. The free-fall time of the compressed region of the cloud is

$$t_{\rm ff} \approx \frac{1}{(G\rho_{\rm cA})^{1/2}}. \tag{2.58}$$

The shock momentum equation in the frame of the shock reads

$$P_1 + \rho_1 v_1^2 = P_2 + \rho_2 v_2^2 \tag{2.59}$$

where the subscript 1 refers to the gas into which the shock is moving, and 2 refers to the gas behind the shock (the shock equations are discussed in more detail in Sect. 3.4). In the limit of a strong shock, P_1 is small compared to $\rho_1 v_1^2$ and $\rho_2 v_2^2$ is small compared with P_2. Thus, for the shock moving through the cloud, in the above notation

$$\rho_{\mathrm{cA}} c_{\mathrm{cA}}^2 \approx \rho_0 v_{\mathrm{s}}^2. \tag{2.60}$$

Combining these results we obtain

$$\frac{t_{\mathrm{dest}}}{t_{\mathrm{ff}}} \approx \frac{3R(G\rho_{\mathrm{c}})^{1/2}}{c_{\mathrm{cA}}}. \tag{2.61}$$

Let λ be the ratio of the cloud radius to its Jeans length before the shock hits:

$$\lambda = \frac{R}{R_{\mathrm{Jeans}}} \approx \frac{R(G\rho_{\mathrm{c}})^{1/2}}{c_{\mathrm{c}}} \tag{2.62}$$

so that

$$\frac{t_{\mathrm{dest}}}{t_{\mathrm{ff}}} \approx 3\lambda \frac{c_{\mathrm{c}}}{c_{\mathrm{cA}}}. \tag{2.63}$$

When this ratio is larger than 1, the cloud can collapse before it is torn apart by the passing shock. Therefore two conditions favor induced star formation in this situation: (1) R is large compared to R_{Jeans}, but if this is true, the cloud will be unstable to collapse even without the shock. Thus for actual induced star formation the quantity 3λ will be of order unity. (2) The cloud cools appreciably after the shock goes through it. If the shock is approximately isothermal, as many types of interstellar shocks are, then $c_{\mathrm{c}} \approx c_{\mathrm{cA}}$ and collapse could be possible. Note that the shock velocity does not appear explicitly in (2.63), but actually it is important because a relatively slow shock allows more time for cooling.

A series of simulations [86, 88, 89, 529] suggests that the supernova trigger is a viable explanation of the existence of at least some of the short-lived radioactive isotopes. The initial condition is a centrally condensed isothermal (10 K) self-gravitating Bonnor–Ebert sphere of 1–2 $M_\odot$, representing a molecular cloud core with mass slightly below its Jeans mass. It is hit by a mild shock wave, at say 25 km/s, which does not shred and destroy the cloud. The idea is that the supernova was far enough away and that there was sufficient intervening interstellar material to slow the shock to this velocity. A supernova can produce both ^{26}Al and ^{60}Fe; the shock could impact a nearby molecular cloud, inducing collapse and injecting some of the ^{26}Al into the collapsing cloud material. The simulations show that a portion of the original cloud material is compressed sufficiently so it becomes marginally unstable to collapse, while the outer regions of the cloud appear to

escape. Thus the general conclusion from such calculations is that in order to get the cloud to collapse, first, it must be fairly close to its Jeans mass anyway, second, the shock must not be too fast nor too slow (5–70 km/s), and third, cooling must be important, so that the layer behind the shock can cool to close to the original cloud temperature.

An important question connected with the shocked cloud is whether the radioactive material behind the shock front actually gets injected into the compressed material that is going to form the star and disk. High-resolution numerical simulations [88, 89, 528, 529] indicate that Rayleigh–Taylor instability occurring at the boundary between the cloud and the external material can mix some of the matter containing supernova-produced radioactivities into the collapsing region. It has not actually been proved that a sufficient amount of radioactive material can be introduced into the inner few AU of the disk, but the results shown in Fig. 2.15 indicate that injection into the collapsing cloud on larger scales does occur.

The main difficulty in the hypothesis of supernova-triggered solar-system formation is that a single supernova does not produce the correct abundance ratios of all of the dozen or so extinct radioactivities that have been detected in meteorites. Thus alternate explanations of the radioactive isotopes have been proposed. At least some of these isotopes could have been produced in the solar nebula itself [463] by energetic particles produced in solar flares impacting dust grains. However the problem is that ^{60}Fe cannot be produced this way; it apparently requires the supernova environment. Energetic particles in the pre-collapse molecular cloud could also produce some of these isotopes. Another variation on the model [401] involves a pre-existing solar nebula disk (rather than a molecular cloud core) which is impacted by a shock from a supernova less than 1 parsec away. If the radioactive isotopes are incorporated into grains of roughly micron size or larger, they could penetrate into the disk. There are other stellar sources besides supernovae that can produce the radioactive isotopes; two important ones are asymptotic giant stars, and massive 60 $M_\odot$ Wolf–Rayet stars. Both of these types of objects can eject the isotopes in stellar winds which can then trigger star formation. Although the supernova trigger is the favored mechanism for the formation of the solar system, the other processes just mentioned could well have made contributions to the radioactive inventory in the meteorites as well.

Expanding HII regions around massive stars could also serve as triggers for star formation. The expansion of an HII region is supersonic with respect to the surrounding cool gas, and it drives a shock, sweeping up the circumstellar gas into a dense shell. The shock precedes the ionization front, and once the shell between them has swept up sufficient mass, it becomes dense and cool, leading to instability and gravitational collapse [162]. The general picture is illustrated in Fig. 2.16. Further work [548] strengthened the case that the fragments that are likely to form in the dense, cool shell will be massive. As such they could generate their own HII regions and initiate a further wave of star formation. Particular examples of star formation observed at the edge of HII regions are Sharpless 104 [133] and RCW79 [570]; an image of the latter region is shown in Fig. 2.17.

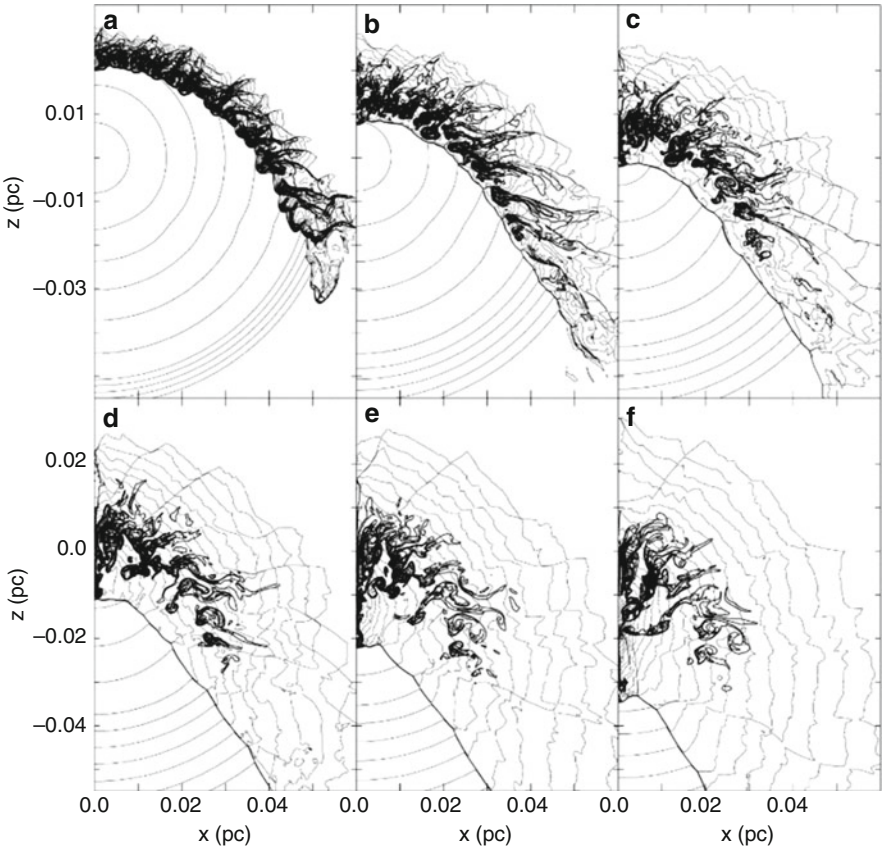

Fig. 2.15 Supernova shock wave hitting a cool cloud of $1\,M_\odot$. The shock is shown at time (**a**) 22,000 years, (**b**) 44,000 years, (**c**) 66,000 years, (**d**) 88,000 years, (**e**) 110,000 years, and (**f**) 132,000 years after it first encounters the cloud. *Thin lines:* contours of equal density, separated by a factor 1.5 in density, with a maximum value of $7.93 \times 10^{-16}\,g\,cm^{-3}$; *thick lines*: contours of equal density of the material behind the shock wave that is being injected into the cloud. The shock-compressed layer is developing a Rayleigh–Taylor instability. The size of one zone in this numerical simulation is 19 AU. The coordinates give the distance scale in units of parsecs on the x- and z-axes. Reproduced by permission of the AAS from [529]. © 2002 The American Astronomical Society

The image was obtained by Spitzer at $8\,\mu m$ and shows that there is a dust ring around the edge of the HII region. The region has been observed at numerous wavelengths. In the millimeter continuum at 1.2 mm a number of dust condensations are observed, practically coinciding with the edge of the HII region. Their masses are 50 to several hundred $M_\odot$. Near infrared photometry and Hα observations show that in the dust condensation near the south-east edge of the HII region there is a compact HII region and several Class I protostars, indicating that a cluster has formed with at least one massive star. There is good evidence that the large HII

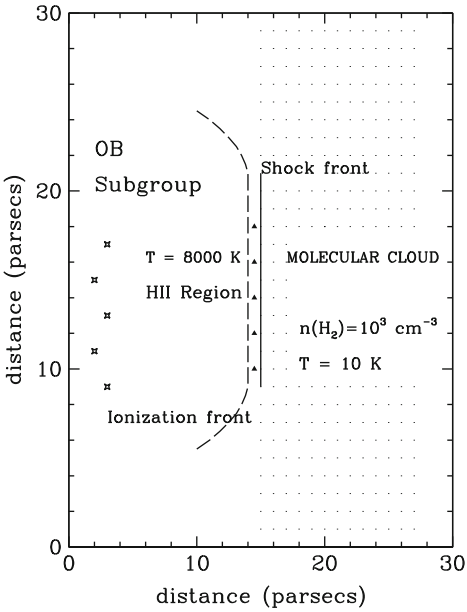

Fig. 2.16 Sketch of the HII region associated with a group of OB stars interacting with a molecular cloud. The stars are originally outside the cloud. After a time of 2 Myr, the ionization front and its preceding shock front have travelled about 10 pc, and the dense layer between them is forced into gravitational collapse, forming new, relatively massive stars. The layer between the shock front and the ionization front has a density of about $n(H_2) \approx 10^5\,\mathrm{cm}^{-3}$ and a temperature of 100 K. The triangles, representing maser sources, infrared sources, or compact continuum sources, are the observed signposts of the massive stars, which themselves are obscured. Once these new stars evolve, their own HII regions can propagate even farther into the cloud, setting off a new wave of star formation, thus inducing a process known as *propagating* star formation. Adapted from [162]

region has expanded into the interstellar medium and swept up a compressed layer of gas and dust between the ionization front and the shock front, and when the layer became massive and dense enough it cooled and fragmented, producing new stars (the "collect and collapse" model). The age of the large HII region is about 1.7 Myr. Analytic models of an expanding HII region in a molecular cloud [548] can be used to deduce that the dense shell fragmented 10^5 years ago, which is consistent with the ages of the protostars and the compact HII region in the clump near the south-east edge.

The numerical simulation of such an expansion [130] with around 10^6 SPH particles showed that an initially uniform-density cloud at 10 K and molecular density $100\,\mathrm{cm}^{-3}$, with an O star turned on at the center, was driven to the point of fragmentation after a time of about 3 Myr, a radius of the HII region of about 10 pc, and a typical fragment mass of $20\dot{M}_\odot$. These findings are fairly consistent with analytical results [548]. The implications of the "collect and collapse" model are that the stars in the daughter cluster, formed in the dense shell, should all have

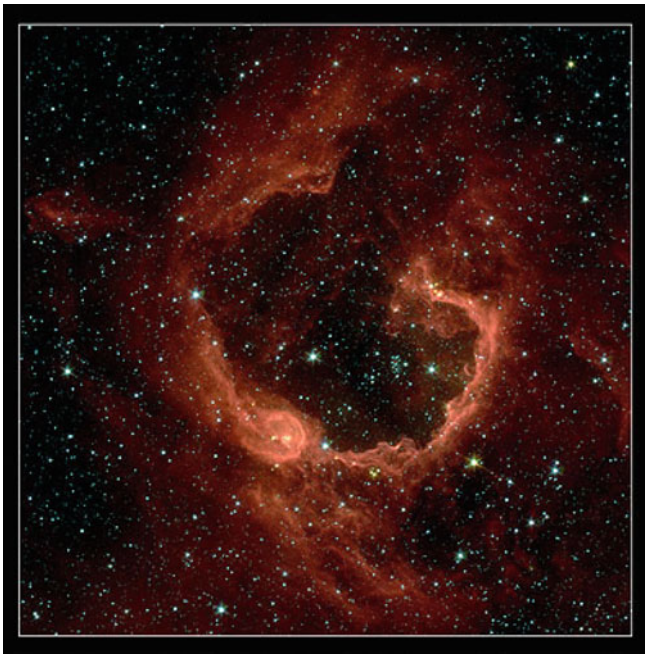

Fig. 2.17 Induced star formation. In the interior of the expanding bubble is an HII region, powered by a massive star. The Spitzer image of RCW79 shown here is taken at 8 μm and indicates emission from dust particles. Two groups of newly-formed stars are suspected to have formed in the dust shell, one near angle 200° relative to the center of the frame, and the other near angle 45°. The radius of the HII region is about 6.4 parsecs. The direction north is up, east to the left. Picture credit: NASA/JPL-Caltech/E.Churchwell [University of Wisconsin-Madison]

about the same age, and that this age should be distinct from that of the original set of stars that generated the HII region. Observational evidence in favor of this picture of propagating star formation has been obtained through estimates of the ages of spatially separated subgroups in an OB star association such as Sco Cen or Orion OB1 [55, 159].

Cloud–cloud collisions, which are generally supersonic, can compress interstellar material and, under the right conditions, induce star formation. It has been suggested [497] that such collisions on the scale of clouds with masses $\approx 5 \times 10^5\,\mathrm{M}_\odot$ could explain the global star formation rate in galaxies, and observational evidence has been found in our Galaxy suggesting that events on these scales have occurred [445]. However, clouds exist on all scales, and numerical simulations of the process typically consider clouds in much lower mass ranges (10–1,000 $\mathrm{M}_\odot$) where numerical issues are less severe. However compression induced by such a collision does not guarantee star formation. For example, if a shock is produced, converting kinetic energy of relative cloud motion into heat, one would expect the cloud to be disrupted if the kinetic energy were on the order of the gravitational binding energy

of one of the clouds. If, however, the heat of compression is radiated away so that the shock is close to isothermal, one would expect that star formation could be possible. However even in this case, early numerical simulations [305] suggested that the clouds needed to be on the verge of Jeans instability for collapse to be induced.

A number of parameters are involved in such a simulation, including the mass ratio of the two clouds, their temperature, the impact parameter in an off-center collision, and the Mach number, which is the ratio of the relative velocity of collision to the post-shock sound speed. The full parameter space has not been explored; however an interesting example is shown in Fig. 2.18. Two clouds of $10\,M_\odot$ each, with radius 0.22 parsec and temperature 35 K, collide off-center with a relative velocity of $1\,km\,s^{-1}$. They are Bonnor–Ebert spheres that are not unstable to collapse. At the initial temperature and density, the interstellar heating/cooling balance (Sect. 2.3) leads to a decrease of temperature on compression; thus after shock compression the material cools down to 10 K, a situation favorable to allowing at least part of the clouds to collapse. The end result, shown in the lower panel of the figure, is a single protostar of mass $0.7\,M_\odot$ and radius 90 AU. The angular momentum of the material provided by the off-center collision results in a disk around the protostar, which develops spiral arms. The fate of the disk is unclear, but it could either fragment, producing a low-mass companion, or simply transport angular momentum outward, allowing disk material to accrete onto the protostar. The mean density of the protostar is $\approx 10^{-13}\,g\,cm^{-3}$ so it is entering the adiabatic collapse phase. A wide range of outcomes is possible with such simulations, from no star formation to formation of several fragments to a binary with a circumbinary disk.

Radiation-driven implosion is a mechanism in which an expanding HII region envelops a dense globule and forces it into collapse by increasing the pressure at the surface [257]. The globules can either be pre-existing or formed by dynamical instabilities generated by the expansion of the HII region into a molecular cloud [159]. Cooling of the compressed cloud material is again key to the forcing of collapse. The heating of the compressed cloud will oppose collapse unless the excess thermal energy is radiated away. Near- isothermal conditions are then favorable for triggering star formation. It would seem counterintuitive for ionizing radiation, which normally tends to disrupt molecular cloud material, to actually aid in generating collapse. But under the right conditions it can happen. For example, numerical simulations [161, 197] of ionizing radiation impinging on a pre-existing turbulent clumpy molecular cloud results in the ionization of the less-dense regions but the compression of the higher-density clumps, producing pillar-like structures similar to those observed, and induced gravitational collapse near the tips of the pillars. A further consequence is an increase in the turbulent kinetic energy in the cloud; thus the ionizing radiation can serve as a driving mechanism (Sect. 2.8). An example of the outcome of a numerical simulation of this process is shown in Fig. 2.19.

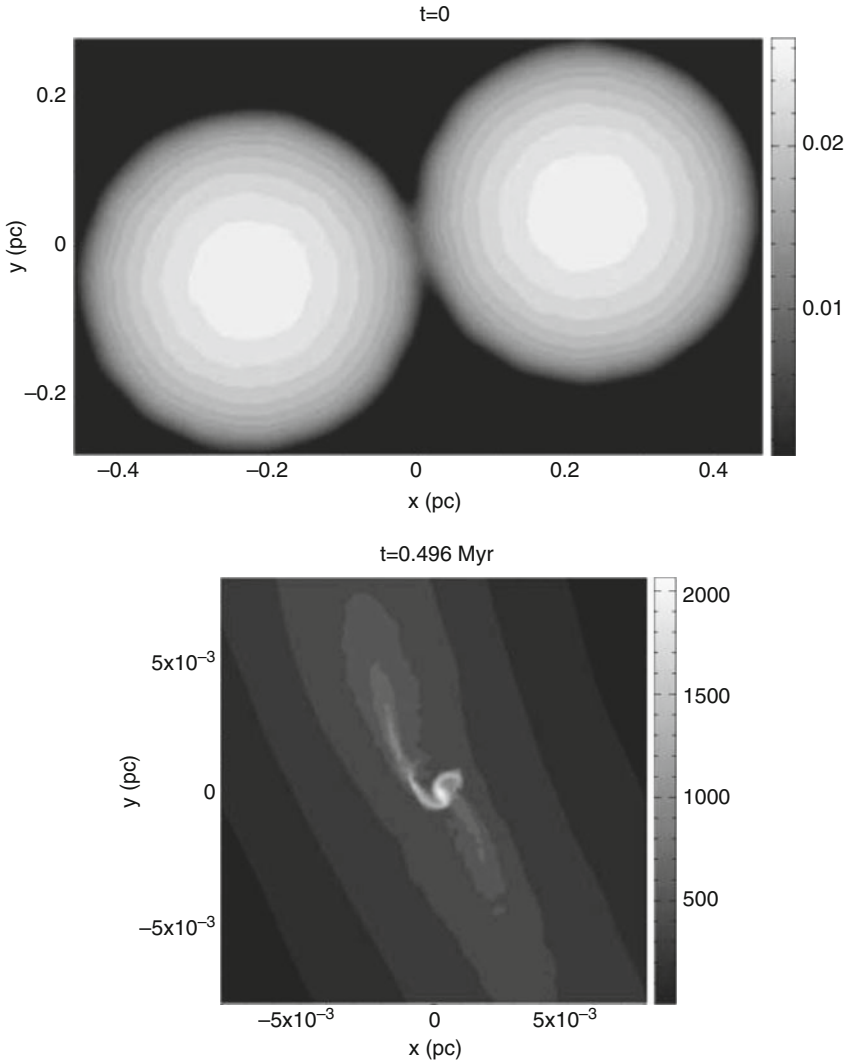

Fig. 2.18 Induced star formation by a cloud–cloud collision calculated with an SPH code in three space dimensions. Two clouds, each with $10\,M_\odot$, collide off-center at 1 km/s. The initial velocity of the clouds is parallel to the x-axis. The upper panel gives the initial condition, and the grey scale gives the column density, integrated along the z-direction, in $g\,cm^{-2}$, ranging from 1.0×10^{-3} to 2.69×10^{-2} in sixteen equal logarithmic intervals. The lower panel (on a greatly reduced scale) shows the star-disk system that has formed after 0.496 Myr, where the logarithmic grey scale ranges from 0.24 to $2.04 \times 10^3\,g\,cm^{-2}$. Reproduced by permission of John Wiley and Sons Ltd. from S. Kitsionas, A. P. Whitworth: *MNRAS* **378**, 507 (2007). © Royal Astronomical Society

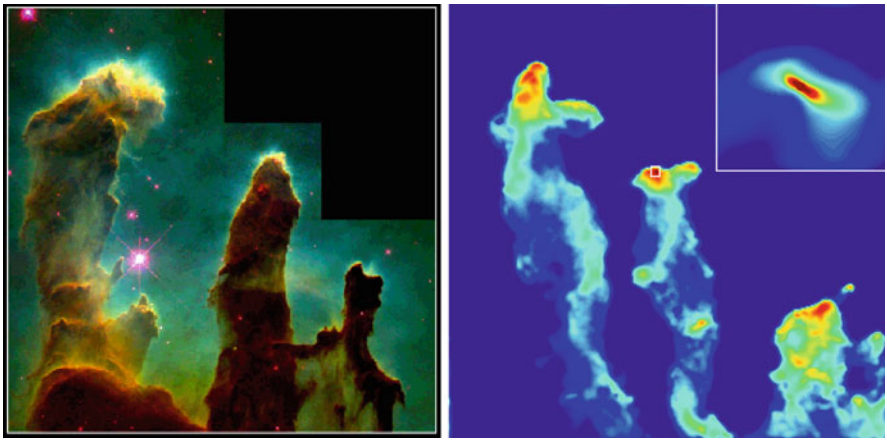

Fig. 2.19 Induced star formation by radiation-driven implosion. *Left:* Optical photograph of the Eagle Nebula (M16). Credit: NASA/ESA/Space Telescope Science Institute/ASU (J. Hester and P. Scowen). *Right:* detail from a three-dimensional numerical (SPH) simulation of ionizing radiation impinging on a clumpy molecular cloud. The surface density ranges from $\log \Sigma = -2.7$ (*red*) to -5.5 (*dark blue*), where Σ is the surface density in $\mathrm{g\,cm^{-2}}$. *Right panel* reproduced by permission of the AAS from [197]. © The American Astronomical Society. The *inset* (not previously published) shows a protostellar disk that has formed in one of the pillars. Composite figure courtesy M. Gritschneder

2.10 Summary

Magnetically controlled star formation. If prestellar cores are magnetically subcritical, that is, they have less mass than the magnetic Jeans mass, they can contract in quasi-equilibrium, and bring the densest central regions to the point of collapse through the process of ambipolar diffusion, which increases the mass-to-flux ratio. The time scale is relatively long, about 10 free-fall times, but it could be shortened in a turbulent region. The main problem with this scenario is that numerous cores have been observed to be supercritical, in which case ambipolar diffusion will still occur but will not control the rate of star formation.

Turbulence-controlled star formation. Observed line widths in interstellar clouds are interpreted in terms of supersonic turbulence. The complicated shock patterns randomly generate highly-compressed regions, which, if they last long enough can reach the point of instability to collapse. On the other hand, on more global scales the turbulence is the primary mechanism that supports most molecular cloud regions against gravitational collapse. The advantage of the turbulence picture is that the time scale for star formation is on the order of 1 Myr, which can explain numerous observations. However, simulations often give efficiencies of star formation that are too high, unless very special properties of the turbulence are assumed. Another problem is that turbulence decays on the time scale of one crossing time, and it has been difficult to identify a mechanism that can continuously regenerate it. Also, the

effects of the magnetic field must be included in numerical turbulent simulations. Nevertheless turbulence is now thought to be the major effect in the determination of the star formation rate and efficiency, and the properties of the resulting stars.
Induced star formation. Supernovae shocks, cloud–cloud collisions, and the sweeping up of dense shells and clumps of gas by massive-star winds and HII regions can induce star formation, and there is considerable observational evidence that these processes occur. Substantial cooling behind shock fronts is a requirement for star formation. It is thought that only a relatively small fraction of the observed star-formation rate can be accounted for by induced processes. However it appears that such an event is necessary to explain the presence in the Solar System of the decay products of extinct radioactive isotopes such as ^{26}Al and ^{60}Fe.

2.11 Appendix to Chap. 2: Note on Numerical Methods

The numerical results discussed in this book, on problems of hydrodynamics and magnetohydrodynamics in 2 or 3 space dimensions, are mostly based on two basic techniques. The first involves expressing the differential equations as finite differences on an Eulerian grid (fixed in space), as discussed, for example, by [435,493]. The second, known as smoothed particle hydrodynamics (SPH), is based on representation of the fluid by a set of particles, each with a given mass, which move around in space under the effect of the various forces involved, such as those from gravity and the pressure gradient. There is no grid, and the method is Lagrangian in nature. The basic properties of the method are reviewed by [368,422]. A direct comparison of the two methods on the same hydrodynamic collapse problem is shown in our Figs. 6.11 and 6.12.

The advancement of physical quantities in time in both cases is based on an *explicit* numerical scheme, in which a quantity at the advanced time t^{n+1} is based entirely on known quantities at the previous time t^n and the assumed time interval Δt. Thus, for a simple example of an equation in one space dimension

$$\frac{\partial y(x,t)}{\partial t} = W(y,x,t) \tag{2.64}$$

where y is a physical variable such as density, the explicit time-differencing scheme would be

$$y(t^{n+1}) = y(t^n) + \Delta t\ W(t^n). \tag{2.65}$$

An alternative to this scheme, known as an *implicit* method, can be written

$$y(t^{n+1}) = y(t^n) + \Delta t\ W(t^{n+1}) \tag{2.66}$$

where generally the solution has to be iterated to self-consistency. This method is used in one-dimensional calculations of stellar evolution.

In any explicit scheme, Δt is limited by two important effects. The first is the Courant–Friedrichs–Lewy (CFL) condition [121] which states that if a grid zone has a width Δx and the fluid is moving through it with a sound speed c_s and a velocity $|v|$, then Δt is limited to a fraction of the crossing time $C_0 \Delta x/(c_s + |v|)$. Here C_0, the Courant number, must be <1 and is usually taken to be about 0.5. The actual time step is taken to be the minimum CFL condition over the entire grid. A numerical instability arises if the condition is not met. In the (gridless) SPH method, the resolution element Δx is replaced by the *smoothing length* h (see below). The second limitation is needed if viscosity, either physical or artificial, is present [see (4.18)–(4.21)]. Then the limit [411] is $\Delta t < (\Delta x)^2/(4\nu)$ where ν is the kinematic viscosity.

In star-formation problems involving collapse from an initially extended configuration of relatively uniform density into a very centrally condensed configuration, a grid-based solution with uniform grid spacing Δx soon becomes inadequate to represent the flow. Much of the mass flows into the central zone and becomes unresolved. Similar problems arise if the computational problem involves fragmentation. The difficulty may be overcome by rezoning the grid in regions that have developed, for example, higher than average density, a procedure known as *adaptive mesh refinement* [50, 256]. The idea is for the code to automatically generate (or delete) finer grids to follow the details of small-scale structures that develop. A three-dimensional zone that needs refinement can be divided into 8 zones, so that the overall spatial resolution is increased by a factor 2. The time-step restrictions must be followed on the refined grid, so that several time steps on a refined grid may be necessary for each time step on the overlying coarser grid. A refined zone can be further refined if needed; in extreme collapse problems, 40 or more levels of refinement are needed if the spatial scale reduction per level, for reasons of accuracy, is limited to a factor 2. For collapse problems, such a procedure is certainly more efficient than providing a single very large uniform grid with the grid spacing needed for the highest-density regions. In SPH calculations, no such refinements are necessary; the spatial resolution is self-adapting as particles move into regions of higher density.

To represent the density or another physical variable in smoothed particle hydrodynamics, one assumes that a particle is not a point mass, but rather a smoothed-out distribution of density over a small volume. Thus, if a particle j momentarily has a position in space $\mathbf{r}_j$, then the contribution of that particle to the overall density at some radius $\mathbf{r}$ is given by

$$\rho_j(\mathbf{r}) = \frac{m_j}{h^3 \pi^{3/2}} \exp[-(|\mathbf{r} - \mathbf{r}_j|/h)^2] \tag{2.67}$$

where m_j is the particle mass and h is the smoothing length. Then the total density at $\mathbf{r}$ is

$$\rho(\mathbf{r}) = \sum_{j=1}^{N} \rho_j(\mathbf{r}). \tag{2.68}$$

Usually N does not have to include the full set of particles, because only close-by particles make a significant contribution to $\rho(\mathbf{r})$. The Gaussian form of the smoothing function is given just as an example; typically the function can have other forms and is cut off at about $2h$. To determine h, which is different for each particle, one requires that the smoothing volume has to include about 50 other particles. Thus regions of higher density automatically develop higher spatial resolution.

The number of zones in a grid-based calculation or the number of particles in an SPH calculation must obey an accuracy requirement known as the Jeans condition [42, 511]. At all points in the domain and at all times the local Jeans length (2.16) must be resolved. In a grid calculation, that means that, locally, there must be at least 4 zones per Jeans length. In SPH, the requirement is that the Jeans length must contain several smoothing lengths. If one ignores this requirement, one runs the risk of observing numerical fragmentation under conditions where physical fragmentation would not occur. If the initial number of particles in an SPH simulation is insufficient to meet this requirement at later times, particle splitting can be employed, with one particle replaced by 8 particles, to improve the resolution.

From the resolution requirement and the CFL condition, it is clear that, for example, in the high-density centers of rapidly collapsing regions, the required time step can be very short, in fact so short that it becomes impossible to follow the simulation for a reasonable amount of time. To deal with this problem, either on a grid [279] or in SPH [41], *sink particles* are introduced. A volume with a given radius is defined (say 1 AU); once the mean density within such a volume exceeds a pre-determined limit, then the volume is replaced by a single particle with the same mass and momentum. Either on a grid or in SPH, the particle is followed as a Lagrangian object, which moves through space under the influence of the gravity of all external matter. The particle can also accrete additional mass and momentum from the surrounding region. Material inside the sink is not resolved; however the sink can be used as a source of energy input from the accretion luminosity of a presumed protostar that has formed within it.

2.12 Problems

1. A spherical cloud of $2\,\mathrm{M}_\odot$ has a uniform density of $5 \times 10^{-19}\,\mathrm{g\,cm^{-3}}$, uniform temperature of 10 K, and uniform composition of molecular hydrogen. It is rotating with uniform angular velocity $\Omega = 2 \times 10^{-14}\,\mathrm{rad\,s^{-1}}$ and is threaded by a uniform magnetic field of 2×10^{-5} Gauss.
   (a) Calculate the gravitational energy, the thermal energy, the rotational energy, and the magnetic energy. Find out if the cloud is unstable to collapse.
   (b) The cloud collapses with conservation of mass, angular momentum, and magnetic flux. How do magnetic energy and rotational energy scale with radius (compare with the scaling of the gravitational energy)? The collapse is isothermal. What happens to the total internal energy?

(c) Will the collapse stop under these assumptions? If so, what stops it and what is the final radius? (Think of physical simplifications).
(d) Is the total energy of the cloud conserved during the collapse? Why?

2. The aim of this problem is to derive the Jeans length in the same way that Sir James Jeans did it, and to identify where a physical inconsistency occurs in this method.

The equations of continuity and momentum are

$$\frac{\partial \rho}{\partial t} + \mathbf{v} \cdot \nabla \rho = -\rho \nabla \cdot \mathbf{v} \tag{2.69}$$

$$\rho \left(\frac{\partial \mathbf{v}}{\partial t} + \mathbf{v} \cdot \nabla \mathbf{v} \right) = -\nabla P - \rho \nabla \phi \tag{2.70}$$

where ρ is the density, P is the pressure, $\mathbf{v}$ is the velocity, and ϕ is the gravitational potential.

Now assume that velocity, density, and ϕ can be represented by a mean state plus a small fluctuation:

$$\rho = \rho_0 + \delta\rho; \quad \mathbf{v} = \mathbf{v_0} + \delta\mathbf{v}; \quad \phi = \phi_0 + \delta\phi. \tag{2.71}$$

Also assume that the mean state is in equilibrium and is isothermal, so $\mathbf{v_0} = 0$, $\partial\rho_0/\partial t = 0$, and $P = c_s^2 \rho$ where c_s is the constant sound speed.

(a) Expand and linearize the equations to get two expressions relating $\delta\rho$ and $\delta\mathbf{v}$.
(b) Then make the simplification that ρ_0 is constant and use the linearized Poisson equation $\nabla^2(\delta\phi) = 4\pi G \delta\rho$ to get an expression for $\delta\rho$ as a function of time

$$\frac{\partial^2}{\partial t^2}(\delta\rho) = \rho_0 \left(4\pi G \delta\rho + \frac{c_s^2}{\rho_0} \nabla^2 \delta\rho \right). \tag{2.72}$$

(c) Now assume that the perturbed density $\delta\rho$ has a plane-wave solution

$$\delta\rho = K' \exp[i(\omega t + kx)] \tag{2.73}$$

where K' is a constant, and find the dispersion relation between ω and k. If ω^2 is positive, the solution is oscillatory. If ω^2 is negative, the disturbance grows exponentially. The critical case corresponds to the Jeans limit. Obtain the Jeans length and the Jeans mass and compare with values obtained by simpler means (using energies, for example).
(d) What is physically inconsistent about the assumptions made?

3. Express (2.10) in terms of velocities: sound velocity, Alfvén velocity, rotational velocity, mean turbulent velocity. Show that the equation for the magnetic Jeans mass is roughly equivalent to the condition that the free-fall time of the sphere be comparable to the crossing time of an Alfvén wave.

4. (a) Use the shock jump conditions for an isothermal shock [(3.37) and (3.38)] to show that the density ratio across the shock is given by the square of the Mach number v_1/c_s, where c_s is constant across the shock.
   (b) A shock is moving at Mach 6 with respect to a spherical clump of radius 2 pc, mass 225 $M_\odot$, and sound speed 0.6 km/s. The shock is isothermal. Would the clump be unstable to collapse before the shock hit it? The gas external to the clump is hotter than that in the clump but in pressure balance with it. What is the Mach number of the shock outside the clump? After the shock hits the clump, calculate the crossing time and the free-fall time of the compressed layer. Is induced star formation likely? What if the shock were Mach 12? Would that make a difference?
5. Consider a uniform-density sphere of radius R, mean column density (particles cm^{-2}) N, particle mass m, uniform magnetic field B, and full-width half-maximum line width ΔV. These are all observable quantities. Make the approximation that the line width arises purely from turbulence.
   (a) Calculate the magnetic energy density (energy per unit volume), the kinetic energy density (in turbulence), and the gravitational energy density in terms of the above quantities.
   (b) Assume a simple model of a cloud core in which all three energy densities are equal. Show that $B \propto (\Delta V)^2/R$; find the constant of proportionality. Assume the cloud is all molecular hydrogen.
   (c) A core in Orion A has a measured line width of 1.7 km s^{-1} in H_2CO, a radius of 0.18 pc, and a measured magnetic field strength $B = 250\,\mu$G. A core in Orion KL has a line width of 2.6 km s^{-1} in NH_3, a radius of 0.047 pc, and $B = 3{,}000\,\mu$G. Do these observations agree with the model or not? For the first case in this problem calculate the column density and the visual extinction (in magnitudes) in the core.
   (d) Show also that, in the model, $B \propto \Delta V n^{1/2}$, where n is the density in particles per cm^3. Does this relation agree with observations?

http://www.springer.com/978-3-642-15062-3

Principles of Star Formation
Bodenheimer, P.
2011, XII, 348 p., Hardcover
ISBN: 978-3-642-15062-3